Performance of Quantum Chemistry Methods for Benchmark Set of Spin–State Energetics Derived from Experimental Data of 17 Transition Metal Complexes (SSE17)

Mariusz Radoń,[*,†] Gabriela Drabik,[‡,†] Maciej Hodorowicz,[†] and Janusz Szklarzewicz[†]

†*Jagiellonian University, Faculty of Chemistry, Kraków, Poland*

‡*Jagiellonian University, Doctoral School of Exact and Natural Sciences, Kraków, Poland*

E-mail: mradon@chemia.uj.edu.pl

Phone: +48 12 6862489

Abstract

Reliable prediction of spin-state energetics for transition metal (TM) complexes is recognized as a challenging and compelling problem in quantum chemistry, with implications for modeling catalytic reaction mechanisms and computational discovery of materials. The computed spin–state energetics are highly variable with the choice of method and credible reference data are scarce, making it difficult to conduct conclusive computational studies of open-shell TM systems. Here, we present a novel benchmark set of first-row TM spin–state energetics, which is derived from curated experimental data of 17 representative complexes containing Fe^{II}, Fe^{III}, Co^{II}, Co^{III}, Mn^{II}, and Ni^{II} with chemically diverse ligands. The reference values of adiabatic or vertical energy differences are derived from spin-crossover enthalpies (9 complexes) or energies of spin-forbidden absorption bands in reflectance spectra (8 complexes).

These are carefully back-corrected for relevant vibrational and environmental effects (due to solvation or crystal lattice) in order to provide the reference values directly comparable with calculated electronic energy differences. The new benchmark set makes it possible to assess the accuracy of spin–state energetics calculated using approximate density functional theory (DFT) and wave function methods with a level of statistical reliability not attained in earlier studies. The lowest mean absolute error (MAE) of 1.5 kcal/mol and maximum error of −3.5 kcal/mol are found for the coupled-cluster CCSD(T) method, which outperforms all tested multireference methods: CASPT2, MRCI+Q, CASPT2/CC and CASPT2+δMRCI. Contrary to earlier claims in the literature, the use of Kohn–Sham instead of Hartree–Fock orbitals in the reference determinant is not found to consistently improve the accuracy of the CCSD(T) spin–state energetics. The best performing DFT methods are double-hybrids (PWPB95-D3(BJ), B2PLYP-D3(BJ)) with the MAEs below 3 kcal/mol and maximum errors within 6 kcal/mol, whereas DFT methods traditionally recommended for spin states (e.g., B3LYP*-D3(BJ) and TPSSh-D3(BJ)) are found to perform much worse with the MAEs of 5–7 kcal/mol and maximum errors beyond 10 kcal/mol. The results of this work are relevant for the proper choice of methods to characterize TM systems in computational catalysis and (bio)inorganic chemistry, and may also stimulate new developments in quantum-chemical or machine learning approaches.

Introduction

Due to their unique electronic structures and resulting properties, transition metal (TM) complexes, as well as TM active sites in metalloproteins and nanoporous materials, are of central importance in various branches of chemistry, biochemistry and materials science.[1] In all these areas, computational studies using quantum chemistry methods play an important role, on par with experiments, to elucidate the properties and reactivities of TM systems.[2–7] But despite unquestionable successes, quantum chemistry methods also face some challenges when it comes to describing the properties of TM complexes with the level of accuracy required in chemical research. One of the biggest chal-

lenges that still remains is to accurately compute *spin-state energetics* (also known as *spin-state splittings*), i.e., the relative energies of the alternative spin states in TM complexes.[6–11]

For mononuclear TM complexes (on which this study is focused), different spin states originate from different distributions of electrons in the manifold of d-orbitals, whose energy levels are split by interactions with the ligands.[1] In first-row TM complexes with electronic configuration d^4–d^8, the low-spin (LS) and high-spin (HS) states may have comparable energies for a certain range of ligand field strengths, and hence the phenomenon of spin crossover (SCO) may occur if the spin–state splitting is small enough to be overcome by the entropic term of the Gibbs free energy.[12–14] If the spin–state splitting is larger, the system may be optically excited to the higher-energy spin state, leading to the occurence of weak, spin-forbidden d–d absorption features.[15–17] The crossing of spin states may also occur along a reaction path, which has significant implications for the mechanisms of spin-forbidden reactions,[18–20] including also examples from enzymatic catalysis[20] and ligand binding to heme.[21,22] Thus, one can find numerous cases in chemical research where accurate computation of spin–state energetics, particularly for first-row TMs, is of critical importance at least in the following aspects: (a) ground state prediction;[23–28] (b) SCO prediction and estimation the transition temperature[29–32] or populations of different spin states for reactive species;[33] (c) interpretation of the electronic spectra[16,17,34,35] and magnetic properties[36,37] of TM complexes; (d) interpretation of the kinetic[22] or thermodynamic[38] features in spin-forbidden reactions.[18]

As mentioned above, accurate computation of TM spin–state energetics is recognized as a grand challenge for quantum chemistry methods. A frequently occurring problem is that different methods lead to divergent and inconsistent results. This behavior is well known for approximate density functional theory (DFT) methods,[9,12,39] but can be observed even for high-level wave function theory (WFT) methods, making it problematic to establish unambiguous reference values.[11,40] For example, the predictions of the singlet–quintet energy gap in $[Fe^{II}(NCH)_6]^{2+}$ (a widely studied, simplified model of SCO compounds) originating from best available diffusion Monte Carlo (DMC)[41,42] and coupled cluster (CC) calculations at the CCSD(T) level[43,44] differ from each other by as much as 20 kcal/mol. Various methods have been advocated in the literature by different au-

thors for the purpose of accurately describing mononuclear TM complexes, e.g., CCSD(T) or its local-correlation approximations,[43–50] multiconfigurational perturbation theory (CASPT2)[51] or its modifications like CASPT2/CC,[52] CASPT2+δMRCI[53] or CASPT2.5,[54] multireference configuration interaction (MRCI+Q),[55] multiconfigurational pair-density functional theory (MC-PDFT),[56,57] density matrix renormalization group (DMRG) and DMRG-based methods[58,59] as well as various Monte Carlo (MC) approaches, including FCIQMC,[60] FCIQMC-tailored distinguishable cluster,[61] AFQMC,[28,62] and DMC.[41,42] It is presently unclear which of these methods yield most reliable spin–state splittings, what are typical error bars of their predictions, whether one should trust more in single- or multi-reference methods and how one should interpret the discrepancies between the results of different methods.[11,28] The difficulty of obtaining indisputably accurate spin–state energetics from theory and the scarcity of reliable benchmark studies significantly impair our ability to carry out conclusive computational studies of open-shell TM systems.

Whereas the majority of theoretical studies attempt to obtain benchmark-quality spin–state energetics from high-level computations (see examples above), we recently focused on the alternative strategy of deriving the reference values from appropriate experimental data.[63,64] As recently reviewed by one of us,[11] the experimental data which are particularly valuable in the context of method benchmarking are: (1) SCO enthalpies and (2) energies of spin-forbidden d–d optical transitions. Out of these it is possible to derive the reference values for, respectively, adiabatic (1) or vertical energy (2) differences between the involved spin states. The best strategy seems to be combining data from the two sources in order to gather in one benchmark set the spin–state energetics of chemically diverse SCO and non-SCO complexes.[11]

Clearly, these ideas are not entirely new. The use SCO data is relatively common in the context of DFT benchmarking, with seminal contributions of Jensen and Cirera[65] and Kepp,[29] followed by Cirera and Ruiz with co-workers,[30,31,66] Vela et al.,[67] Ohlrich et al.,[68] and Mariano et al.[69] The use of spin-forbidden d–d transition energies has been pioneered by Hughes and Friesner,[70] who also pointed out that these spectral data allow to probe a more diverse range of ligand field strengths and TMs than is available from the SCO data. Some SCO or non-SCO experimental data have also

been used occasionally for testing the accuracy of selected WFT methods (see references in our review[11]). Still, these ideas have not received enough attention in the literature—particularly with regard to the joint use of SCO and non-SCO data, assessing the accuracy of WFT and DFT methods simultaneously on one common benchmark set, and taking into account appropriate corrections for vibrational and environmental effects—before our first benchmark study of four octahedral Fe complexes[63] and subsequent study of metallocenes.[64] One obvious limitation of the mentioned studies, which we would like to eliminate now, was the small number of studied complexes, leading to potential concerns about the representability of these benchmarks.

In this work we develop a novel benchmark set of spin–state energetics (SSE17), which is based on the experimental data of 17 first-row TM complexes: enthalpy differences for 9 SCO complexes (**A1**–**A9**) and spin–forbidden absorption maxima for 8 non-SCO complexes (**B1**–**B4**, **C1**–**C4**). The molecular structures of all complexes are shown in Figure 1. The present set of TM complexes is not only larger than in the previous studies,[63,64] but also more balanced considering the diversity of TM ions (Fe^{II}, Fe^{III}, Co^{II}, Co^{III}, Mn^{II}, Ni^{II}), ligand-field strength and coordination architectures. The most important class of Fe^{II} SCO complexes is decently represented by 5 items (**A2**–**A6**), but does not dominate the entire set as we also include SCO complexes of Fe^{III} (**A1**), Co^{II} (**A7**), Ni^{II} (**A8**), and Mn^{II} (**A9**). Non-SCO complexes with LS ground state (**B1**–**B4**) and HS ground state (**C1**–**C4**) are evenly represented, accounting for the range of strong and weak ligand fields, in which the most common singly spin-forbidden transitions are observed: Fe^{II} doublet–quartet (**B1**), Fe^{II} and Co^{III} singlet–triplet (**B2**–**B4**), Fe^{III} and Mn^{II} sextet–quartet (**C1**–**C3**), and Fe^{II} quintet–triplet (**C4**). The selection of complexes is dictated by the availability of credible experimental data and the possibility of performing most expensive WFT calculations, including canonical CCSD(T). The latter condition, with our recently developed protocols to efficiently estimate the complete basis set (CBS) limit,[71] presently restricts the molecular size to ca. 50 atoms.

When deriving electronic spin–state splittings from the experimental data, it is necessary to back-correct for vibrational and environmental corrections, which can reach up to several kcal/mol in magnitude.[11] The vibrational correction originates from the change of vibrational frequencies

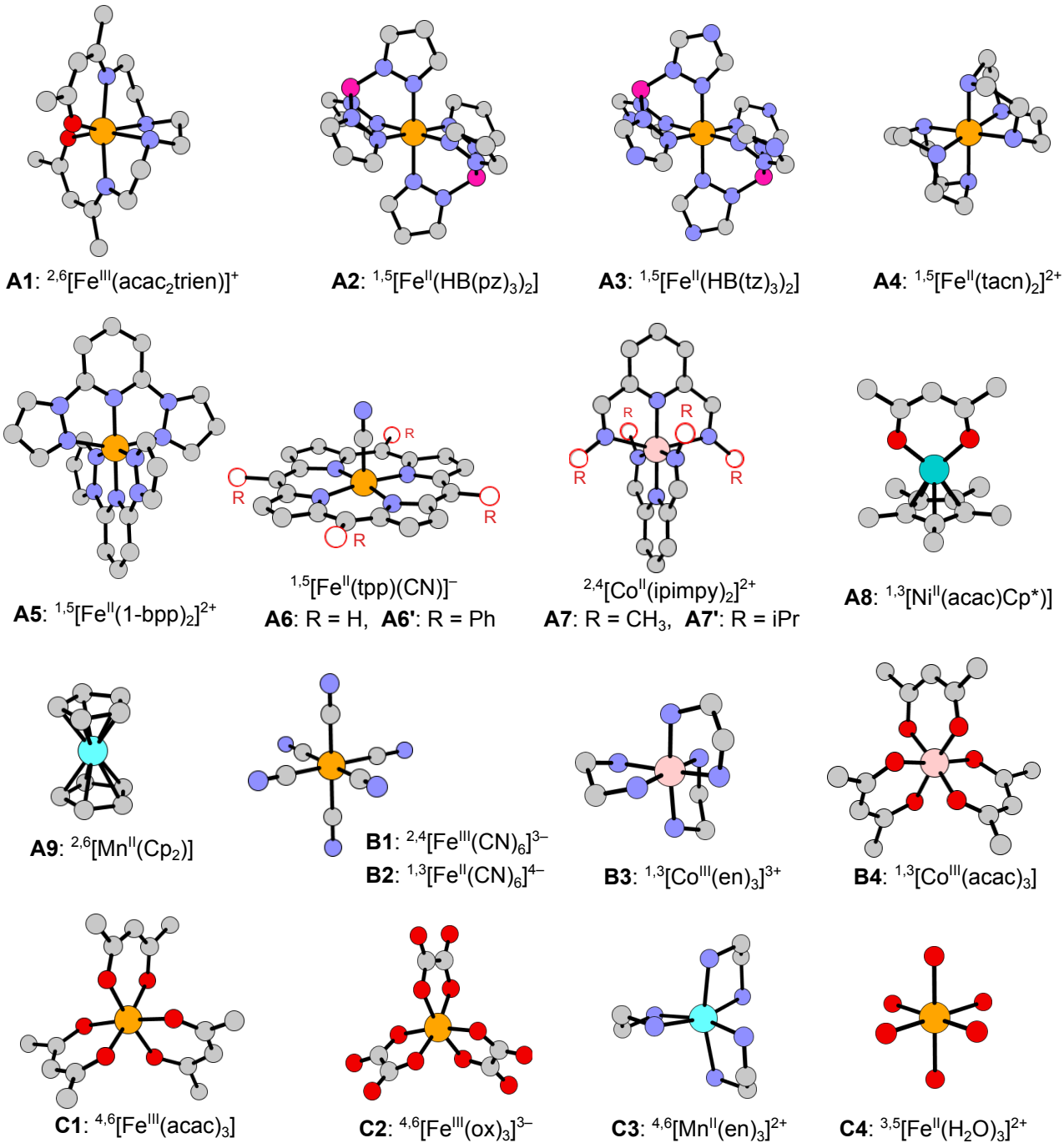

Figure 1: Molecular structures of 17 complexes studied in this work (hydrogens omitted for clarity): **A1**–**A9** SCO complexes, **B1**–**B4** complexes with LS ground state, **C1**–**C4** complexes with HS ground state. Multiplicities of the considered spin states are given in the superscript. Ligand abbreviations: $acac_2$trien = dianion of Schiff base obtained from the 1:2 condensation of acetylacetone with triethylenetetramine; $HB(pz)_3$ = hydrotris(pyrazol-1-yl)borate; $HB(tz)_3$ = hydrotris(1,2,4-triazol-1-yl)borate; tacn = 1,4,7-triazacyclononane; 1-bpp = 2,6-di(pyrazol-1-yl)pyridine; tpp = tetraphenylporphyrin; ipimpy = 2,6-bis(isopropyliminomethyl)pyridine; acac = acetylacetonate; Cp = cyclopenadienyl; Cp* = pentametylcyclopentadienyl; en = etylenediamine; ox = oxalate.

with the change of spin state. The environmental correction describes the effect of solvation or crystal packing on the investigated spin–state splitting as compared with that of isolated molecule. We use state-of-the-art approaches for estimating both types of correction. We now also introduce some improvements related to evaluation of these corrections and the usage of experimental data. Firstly, wherever possible we now include data for SCO complexes in multiple environments, i.e., crystal and solution or solutions in different solvents, in order to obtain more reliable averaged back-corrected values and estimate the uncertainty related to determination of the environmental correction from the spread of different back-corrected values. Secondly, employing the vibronic simulation approach introduced in ref 64, we now include the vibrational correction also for vertical transitions, which leads to more balanced treatment of non-SCO and SCO data. Thirdly, with the aim of avoiding large environmental corrections previously observed for vertical energies in ionic complexes,[63] we now use reference geometries optimized within a charge-screening model as they are closer to experimental condensed-phase geometries.[72] Finally, recognizing pronounced sensitivity of vertical excitation energies to the quality of molecular geometries[64] and the difficulty of computing these geometries with sufficient accuracy for TM complexes in solution, we now decided to include only the data of spin-forbidden d–d transitions measured for solid-state compounds with known crystal structures. For such cases, the experimental crystal structure will be directly used to calculate the environmental correction, hereby alleviating the mentioned sensitivity problem. We use diffuse reflectance spectroscopy[73] to measure spin–forbidden d–d transitions for complexes **B1**–**B4**, **C1**–**C4** in solid state. To satisfy the constrain of having simultaneously the spectra and crystal structures available for identical solid-state compounds and recognizing to the scarcity of appropriate data in the literature, we decided, specifically for developing the SSE17 benchmark set, to record most of the required reflectance spectra and to obtain a crystal structure of a new compound $[Mn(en)_3]Cl_3 \cdot H_2O$ (**1**) containing HS Mn^{II} complex **C3**.

This paper is organized as follows. After presenting some necessary methodology details, the Results and Discussion section describes in detail the SSE17 benchmark set, including the experimental data and applied corrections, based on which the reference spin–state splittings are derived.

The SSE17 reference data are subsequently used to benchmark the accuracy of selected WFT and DFT methods, hereby providing us with statistically relevant conclusions on the performance of various quantum chemistry methods for spin–state energetics of first-row TM complexes.

Computational and Experimental Methods

DFT Calculations

Geometry Optimizations

Geometries of complexes comprising the SSE17 set were optimized at the PBE0[74]-D3(BJ)[75]/def2-TZVP[76] level within the COSMO model[77] ($\varepsilon = \infty$) using Turbomole v7.5.[78,79] Both spin states were optimized for SCO complexes (**A1**–**A9**) or only the ground state for others (LS for **B1**–**B4**, HS for **C1**–**C4**). Jahn–Teller (JT) geometry distortions in degenerate electronic states were accounted for by properly reducing the computational symmetry, where applicable. It has been verified by running frequency calculations that the optimized geometries are energy minima (or very close to them for **A9**, see Supporting Information).

Single-Point Energy Calculations

Employing the optimized COSMO/PBE0-D3(BJ)/def2-TZVP geometries (see above), subsequent single-point calculations in vacuum were performed using 32 DFT methods (for the list of functionals, see Results and Discussion) including dispersion corrections wherever available. The basis set was chosen as def2-QZVPP for double-hybrid functionals or def2-TZVPP for others. The energies reported below include additive corrections for scalar-relativistic effects at the second-order Douglas–Kroll (DK) level.[80] Depending on the choice of functional, the calculations were performed using either Turbomole,[78,79] Gaussian 16[81] or Orca v5.0.[82,83] More details can be found in Supporting Information.

WFT Calculations

Single-Point Energy Calculations

Employing the optimized COSMO/PBE0-D3(BJ)/def2-TZVP geometries (see above), single-point calculations in vacuum were performed with selected WFT methods. Single-reference coupled-cluster (CC) calculations were performed at the CCSD(T) level employing Hartree-Fock (HF) orbitals in the reference Slater determinant. Alternatively, KS-CCSD(T) calculations were performed employing Kohn-Sham (KS) orbitals in the reference determinant; we compared the PBE0 and PBE orbitals, leading to methods abbreviated as PBE0-CCSD(T) and PBE-CCSD(T). The CC calculations for open-shell systems utilized the ROHF/UCCSD(T) formulation.[84,85] Among multireference methods we used CASPT2 (IPEA shift 0.25 a.u.), CASPT2/CC,[52] CASPT2+δMRCI,[53] and MRCI+Q in Celani–Werner internally-contracted formulation.[86] The calculations were performed using Molpro,[87,88,89] except for CASPT2 calculations performed using OpenMolcas.[90] All valence electrons and TM 3s3p electrons were correlated.

Basis Sets and Approaching Complete Basis Set (CBS) Limit

In order to efficiently approach the CBS limit in the CCSD(T) calculations, we employed our recently developed CCSD(T#)-F12a protocol,[71] which is based on the explicitly-correlated CCSD-F12a theory of Werner with co-workers,[91] but uses a modified scaling of the perturbative triples. In the benchmark study of small TM complexes, the CCSD(T#)-F12a method in combination with a relatively small basis set cT(D), which is composed of cc-pwCVTZ for TM atom, cc-pVTZ for ligand atoms directly bound to TM atom and cc-pVDZ for the remaining ligand atoms, has been shown to reproduce the CCSD(T)/CBS limits of relative spin–state energetics to within 1 kcal/mol (mean deviation 0.2, mean absolute deviation 0.4, maximum deviation 0.8 kcal/mol).[71] Following this strategy, the best estimates of the CCSD(T) energies in the CBS limit were calculated as

$$\Delta E_{\text{final}}^{\text{CCSD(T)}} = \Delta E_{\text{cT(D)}}^{\text{CCSD(T\#)-F12a}} + \Delta(\text{DK})^{\text{CCSD(T)}}, \quad (1)$$

where the last term is correction for scalar-relativistic effects at the second-order DK level, obtained from conventional CCSD(T) calculations

$$\Delta(\mathrm{DK})^{\mathrm{CCSD(T)}} = \Delta E^{\mathrm{CCSD(T)}}_{\mathrm{cT(D)\text{-}DK}} - \Delta E^{\mathrm{CCSD(T)}}_{\mathrm{cT(D)}}. \quad (2)$$

The cT(D)-DK basis set is DK-recontraction of the cT(D). Calculations with the remaining WFT methods were performed using the cT(D)-DK basis set and resulting energy difference were corrected to the CBS limit of each method based on the observed[71] excellent transferability of the basis set incompleteness error between CCSD(T) and other WFT methods, i.e.

$$\Delta E^{\mathrm{method}}_{\mathrm{final}} = \Delta E^{\mathrm{method}}_{\mathrm{cT(D)\text{-}DK}} + \Delta E^{\mathrm{CCSD(T)}}_{\mathrm{final}} - \Delta E^{\mathrm{CCSD(T)}}_{\mathrm{cT(D)\text{-}DK}}. \quad (3)$$

Full computational details can be found in Supporting Information.

Choice of Active Space in Multireference Calculations (CASPT2, MRCI)

Based on Pierloot's rules for mononuclear TM complexes,[92,93] the set of active orbitals was chosen to include: (a) five valence TM 3d orbitals, (b) one or two mostly doubly-occupied ligand orbitals considerably overlapping with the TM 3d orbitals to form covalent metal-ligand combinations, and (c) up to five mostly virtual orbitals with the TM 4d character to describe the double–shell effect, in some complexes jointly with π-backdonation. The resulting active space of 10–12 orbitals is regarded as the standard choice for octahedral complexes[52,63,94,95] as it reasonably accounts for metal–ligand covalency and double-shell effects. A slightly larger active space of 14 active orbitals was chosen for organometallic complex **A8** following the work of Pierloot et al.[96] Detailed description of the active spaces can be found in Supporting Information (Table S6).

Experimental Procedures

Diffuse Relectance Spectra Evidencing Spin-Forbidden d–d Transitions

Diffuse reflectance spectra were measured in slow mode on a Shimadzu UV-3600 UV-VIS-NIR spectrophotometer equipped with ISR-260 integrating sphere attachment. The $BaSO_4$ (Shimadzu, spectroscopic grade) was used as the reference. Samples were prepared by mixing crystalline compound with a small amount of $BaSO_4$ and grated in an agate mortar. Gaussian analysis of the spectra was performed to locate the maxima of overlapping bands (see Supporting Information). The $Fe(acac)_3$, $Co(acac)_3$ and $K_3[Fe(ox)_3]\cdot 3H_2O$ were synthesized as described in literature and recrystallized twice prior to use. $K_4[Fe(CN)_6]\cdot 3H_2O$ (p.a.) was from Aldrich.

Synthesis and Crystal Structure of $[Mn(en)_3]Cl_2\cdot H_2O$, (1).

Ethylenediamine (en), Sigma-Aldrich, p.a., was kept with solid NaOH for one week under argon and than distilled under argon prior to use. 0.1 g (0.51 mM) of $MnCl_2\cdot 4H_2O$ was placed in glass vial and 3 mL of freshy distilled en was added under argon. The vial was sealed with a torch and kept at ca. 90 °C (water bath) for ca. one month. The vial was then cooled to room temperature and the formed colorless crystals were taken off for X-ray crystal structure analysis and reflectance spectra measurements. The crystals for the X-ray analysis were covered with apiezone to avoid decomposition, while for the reflectance spectra the crystals were dried with filtration paper prior to the measurements. The rest of the crystals were filtered off, washed with water and a small amount of MeOH. All manipulations were performed under argon. Anal. calcd for $\mathbf{1}\cdot 0.5\,MeOH\cdot 1.5\,H_2O$: C, 21.26; N, 22.89; H, 8.51%. Found: C, 21.36; N, 23.23; H, 8.085 %. The X-ray crystal structure analysis was performed at 250 K using the MoKα radiation, with full details described in Supporting Information. CCDC 2259710 contains additional crystallographic data.

Results and Discussion

Benchmark Set of Spin–State Energetics (SSE17)

The presently reported SSE17 benchmark set of spin–state energetics is derived from experimental data of 17 complexes (**A1**–**A9**, **B1**–**B4**, **C1**–**C4**), whose structures are shown in Figure 1. Following the general idea introduced in our previous studies,[11,63,64] we derive the reference value of the adiabatic spin–state splitting (ΔE_{ad}) for each SCO complex (**A1**–**A9**) from the experimental enthalphy difference (ΔH), whereas for each of the remaining complexes (**B1**–**B4**, **C1**–**C4**) we derive the reference values of the vertical spin–state splitting (ΔE_{ve}) from the experimental energy of the lowest, singly spin-forbidden d–d absorption maximum (ΔE_{max}). In both cases, the raw experimental value ($\Delta E_{\mathrm{exptl}}$, i.e., either ΔH or ΔE_{max}) is back-corrected for relevant vibrational (δ_{vibr}) and environmental (δ_{env}) effects in order to provide the reference value of the corresponding, purely electronic energy difference (ΔE_{ref}, i.e., either ΔE_{ad} or ΔE_{ve}):

$$\Delta E_{\mathrm{ref}} = \Delta E_{\mathrm{exptl}} - \delta_{\mathrm{vibr}} - \delta_{\mathrm{env}} - \delta_{\mathrm{subst}}. \tag{4}$$

In addition, for **A6** and **A7**, which are simplified models of the actual complexes studied experimentally (**A6′**, **A7′**), we also back-correct for the effect of ligand's side substituents (δ_{subst}) present in the actual complex, but simplified to H atoms in the model; for other complexes the δ_{subst} term is zero by definition. Below, we discuss the experimental data and applied corrections (δ_{vibr}, δ_{env}, δ_{subst}) leading to determination of the SSE17 dataset, which is summarized in Table 1. Full details of calculating the δ-corrections are given in Supporting Information.

Note that all energy differences between spin states are consistently defined under the following sign convention (which also applies to the δ-corrections):

$$\Delta E = E(\text{higher-spin}) - E(\text{lower-spin}). \tag{5}$$

Thus, $\Delta E < 0$ for complexes with HS ground state (**C1**–**C4**).

Table 1: The SSE17 Benchmark Set: Experimental Data, Applied Corrections, and Reference Values of Electronic Energy Differences. [a]

	complex [b,c]	type [d]	environ.[e]	ΔE_{exptl} [f]	δ_{env}	δ_{vibr}	δ_{subst}	ΔE_{ref}
A1	$^{2,6}[Fe^{III}(acac_2trien)]^+$	ad	CH_2Cl_2	1.7 [97]	0.5	−1.2		3.0(7) [g]
			acetone	2.0 [97]	0.8	−1.2		
			MeCN	2.4 [97]	0.8	−1.2		
			MeOH	3.1 [97]	0.8	−1.2		
			THF	3.4 [97]	0.9	−1.2		
A2	$^{1,5}[Fe^{II}(HB(pz)_3)_2]$	ad	$CHCl_3$	5.7 [98]	−0.2	−1.0		6.9
A3	$^{1,5}[Fe^{II}(HB(tz)_3)_2]$	ad	crystal [h]	3.8 [99]	−0.5	−1.0		5.3
A4	$^{1,5}[Fe^{II}(tacn)_2]^{2+}$	ad	water	5.7 [100]	2.4	−1.6		4.7(5) [g]
			MeCN	5.0 [101]	1.8	−1.7		
			DMF	5.0 [101]	2.4	−1.7		
A5	$^{1,5}[Fe^{II}(1\text{-bpp})_2]^{2+}$	ad	crystal [i]	4.1 [102]	−0.4	−1.1		5.2(4) [g]
			acetone	5.8 [103]	2.0	−1.1		
A6	$^{1,5}[Fe^{II}(tpp)(CN)]^-$	ad	crystal [j]	3.2 [104]	0.0	−0.8	−0.1	4.8
A7	$^{2,4}[Co^{II}(ipimpy)_2]^{2+}$	ad	crystal [k]	2.4 [105]	1.3	−1.0	−0.9	3.0(1)
			acetone	2.4 [105]	1.1	−0.8	−0.9	
A8	$^{1,3}[Ni^{II}(acac)(Cp^*)]$	ad	toluene	2.7 [106]	−0.2	−0.3		3.2
A9	$^{2,6}[MnCp_2]$	ad	toluene	3.1 [107]	0.2	−1.3		4.2
B1	$^{2,4}[Fe^{III}(CN)_6]^{3-}$	ve	crystal [l]	58.0 [t, 108]	−0.4	−2.3		60.7
B2	$^{1,3}[Fe^{II}(CN)_6]^{4-}$	ve	crystal [m]	68.0 [t]	−3.5	−2.9		74.5
B3	$^{1,3}[Co(en)_3]^{3+}$	ve	crystal [n]	39.5 [t]	−0.6	−2.1		42.1
B4	$^{1,3}[Co(acac)_3]$	ve	crystal [o]	26.0 [t]	1.5	−1.8		26.4
C1	$^{4,6}[Fe(acac)_3]$	ve	crystal [p]	−27.4 [t]	1.9	−0.2		−29.1
C2	$^{4,6}[Fe(ox)_3]^{3-}$	ve	crystal [q]	−30.3 [t]	2.2	−0.2		−32.3
C3	$^{4,6}[Mn(en)_3]^{2+}$	ve	crystal [r]	−45.2 [t]	0.0	−1.6		−43.5
C4	$^{3,5}[Fe(H_2O)_6]^{2+}$	ve	crystal [s]	−37.2 [t]	1.0	−0.2		−38.0

[a] All values in kcal/mol. [b] Superscript gives multiplicities of the considered spin states. [c] For ligand abbreviations see caption of Figure 1. [d] Type of energy difference: adiabatic (ad) or vertical (ve). [e] Molecular environment, i.e. solvent or crystal, in which experimental data were obtained. [f] Raw experimental value: enthalpy difference ΔH for adiabatic energies of complexes **A1**–**A9** or energy corresponding to band maximum position ΔE_{max} for vertical spin-forbidden transitions in complexes **B1**–**B4**, **C1**–**C4**, with reference to the source of data. [g] For complexes characterized in multiple environment, the assumed reference value is the mean of different back-corrected values, the uncertainty estimate is based on the maximum deviation of back-corrected values from the mean. [h] $[Fe(HB(tz)_3)_2]$, refcode BAXFIS[01].[99] [i] $[Fe(1\text{-bpp})_2](BF_4)$, refcode XENBEX03.[102] [j] [K(222)][Fe(tpp)(CN)], refcode QOVKIW[03].[109] [k] $[Co(ipimpy_2)(ClO_4)_2]$, refcode IQICEQ.[110] [l] $K_3[Fe(CN)_6]$, ICSD 60535.[111] [m] $K_4[Fe(CN)_6]\cdot 3H_2O$, refcode XUNNAX.[112] [n] $[Co(en)_3]Cl_3$, refcode IRIRAC.[113] [o] $[Co(acac)_3]$, refcode COACAC03.[114] [p] $[Fe(acac)_3]$, refcode FEACAC05.[115] [q] $K_3[Fe(ox)_3]\cdot 3H_2O$, refcode KALGOU.[116] [r] $[Mn(en)_3]Cl_3\cdot H_2O$, CCDC 2259710 (this work). [s] $[Fe(H_2O)_6](NH_4)_2(SO_4)_2$, ICSD 14346.[117] [t] This work.

SCO Complexes (A1–A9)

The reference experimental value is the molar enthalpy of the SCO process (ΔH), which we use to derive the adiabatic electronic energy difference between the involved spin states (ΔE_{ad}). All the experimental ΔH values were taken from the literature (see references in Table 1). These values originate either from calorimetric measurements (for **A3** and **A5** in crystal) or thermodynamic analysis of temperature-dependent spin equilibria (e.g., fitting magnetic susceptibility or magnetic resonance data as a function of temperature). Note that for all considered SCO complexes, the observed transitions are single-step and without hysteresis, making it straightforward to relate the observed ΔH to the underlying ΔE_{ad} of the spin-transiting molecule.

The vibrational correction (δ_{vibr}) needed to relate the ΔH and ΔE_{ad} values accounts for the difference in zero-point energies (ZPEs) and thermal vibrational energies between the two spin states.[11] It was computed based on DFT frequencies using a well-known expression from statistical thermodynamics (see eq. (S.8), Supporting Information), which is based on the harmonic oscillator model. The δ_{vibr} corrections are within 2 kcal/mol in magnitude and uniformly negative (cf Table 1) due to the lowering of metal–ligand vibrational frequencies upon the LS→HS transition.[118,119]

The environmental correction (δ_{env}) describes the influence of the environment (solution or crystal) on the ΔE_{ad} value. This correction was computed depending on the experimental conditions under which a given SCO complex has been characterized. For complexes characterized in solution (**A1**, **A2**, **A4**, **A5**, **A7**–**A9**), the δ_{env} correction was determined using COSMO/DFT calculations with the dielectric constant corresponding to actual solvent used in the experiment. In addition, when considering complexes (**A1** and **A4**) that contain solvent exposed N–H groups, which are potential H-bond donors, in solvents that are potential H-bond acceptors (acetone, MeCN, MeOH, THF, DMF, water), we added explicit solvent molecules to attain a more realistic description (for details, see Supporting Information). As might be expected, the δ_{env} corrections are negligible in non-polar solvents such as toluene, but become more important in polar solvents, especially when H-bonding is operative. For SCO complexes characterized in solid state (**A3**, **A5**–**A7**), the δ_{env} correction was determined from periodic DFT+U calculations using a similar

methodology as recently described by Vela with co-workers,[67] which is detailed in Supporting Information. The δ_{env} corrections due to crystal packing are within 1.5 kcal/mol, sometimes negligible (**A6**). However, the present sample of solid-state SCO complexes is too small to draw general conclusions about the role of crystal packing effects, which are known to be much larger in certain cases.[11,120] Also note that the present definition of δ_{env} term is slightly different from that of Vela et al.,[67] who assumed for isolated complexes geometries excised from respective crystal models, whereas in the present definition these are the COSMO/PBE0-D3(BJ)/def2-TZVP geometries, identical with those used in subsequent single-point WFT and DFT calculations.

The substituent correction (δ_{subst}) for complexes **A6** and **A7** was quantified using dispersion-corrected DFT calculations (Supporting Information). A negligible δ_{subst} value is obtained for **A6** showing that Ph side substituent of the porphyrin ring present in **A6′**, but replaced with H atoms in **A6**, have almost no effect on the singlet–quintet splitting. This is similar to the previous case of triplet–quintet splitting in [Fe^{II}(tpp)].[120] Note, however, that larger substituent effects have beeen observed in other metalloporphyrins.[120] Moreover, ligand's substituents may indirectly influence spin–state energetics through the crystal packing effect (which is obviously included in the δ_{env} correction, calculated here with full ligand representation). In the case of **A7**, the δ_{subst} correction (due to simplification of the iPr groups in **A7′** to CH_3 groups in **A7**) is ca. 1 kcal/mol.

Non-SCO Complexes (B1–B4, C1–C4)

The reference experimental value is position of the absorption maximum of a spin-forbidden d–d transition, translated to energy units

$$\Delta E_{\text{max}} = \pm hcN_A\tilde{\nu}_{\text{max}}, \tag{6}$$

where $\tilde{\nu}_{\text{max}}$ is the wave number at the band maximum position, h is the Plack constant, c the velocity of light, N_A the Avogadro constant. The sign $\pm$ is chosen for complexes with LS or HS ground state, respectively, due to the sign convention (5). We use the ΔE_{max} values obtained from

experimental spectra (more of which latter) to derive vertical energy differences (ΔE_{ve}) between the pairs of involved spin states. Note that for the purpose of developing the SSE17 dataset, we are only interested in the lowest-energy, singly spin-forbidden d–d transitions, i.e.: doublet–quartet for LS d^5 complex **B1**; singlet–triplet for LS d^6 complexes **B2**–**B4**; sextet–quartet for HS d^5 complexes **C1**–**C3**; and quintet–triplet for HS d^6 complex **C4**. The corresponding bands are straightforward to assign based on Tanabe–Sugano diagrams [15,121,122] (see Figure S9, Supporting Information).

The vibrational correction (δ_{vibr}) accounts for the difference between the absorption maximum and the underlying vertical excitation energy, i.e., deviation from the vertical energy approximation. [64,123,124] The δ_{vibr} term was quantified from simulations of the vibrational progression of the d–d transition within the Franck–Condon approximation, following the approach introduced in our previous work [64] and detailed in Supporting Information. As can be seen from Table 1, the resulting vibronic corrections to vertical energies are uniformly negative (under the sign convention (5)) and their magnitudes range from negligible for some HS complex up to 2–3 kcal/mol in the case of LS complexes. These δ_{vibr} corrections have good correlation with the ZPE differences between the spin states (Table S8, Supporting Information), suggesting [11,124] that the main physical effect responsible for deviation from the vertical energy approximation is the change of vibrational frequencies upon the spin transition.

The environmental correction (δ_{env}) describes the effect exerted on the ΔE_{ve} value by the molecular environment in which the optical spin-transition is measured. Being aware from previous studies [11,34,64,125] that d–d vertical excitation energies are very sensitive to assumed molecular geometries, and that the latter ones are difficult to computationally predict with sufficient accuracy (especially for TM complexes in solution), we decided to include in the SSE17 benchmark set only complexes for which the d–d bands have been characterized for solid-state compounds with known crystal structures. The availability of the crystal structure evidences not only the geometry of ligh-absorbing TM complex, but also its molecular environment in the second coordination sphere, both of which may influence the vertical excitation energy. Both types of structural information are also not easily available for TM complexes in solution, which is why we intentionally do not consider

any solution-state data of d–d transitions in the construction of the SSE17 benchmark. The use of arbitrary computed geometries without a proper backup from the experimental crystal structures could easily lead to significant and uncontrollable errors in calculated vertical energies, which is precisely what we would like to avoid in developing the benchmark set.

To determine the δ_{env} correction for a spin-excitation in solid state, a cluster model of each light-absorbing TM complex was constructed based on the experimental crystal structure of the actual compound used in the measurements (see footnotes under Table 1 for references). The cluster model was composed of a single TM complex surrounded by its neighboring counterions (treated quantum-mechanically), whereas the interaction with the remaining ions present in the crystal lattice was described by the Ewald potential (electrostatic embedding).[126] For non-ionic complexes **B4** and **C1**, the cluster model was limited to a single TM complex in its crystalline geometry. Details of the cluster models can be found in Supporting Information. The environmental correction δ_{env} was obtained as the difference between two vertical excitation energies calculated at the CASPT2 level: one for the cluster model, another for isolated TM complex in vacuum using its COSMO/PBE0-D3(BJ) geometry, i.e., the same one as adopted in subsequent single-point WFT and DFT calculations. Such definition of the δ_{env} term (a) utilizes geometry information from the experimental crystal structure and (b) ensures consistency between the geometry adopted in the single-point calculations and the reference value (resulting from subtraction of the δ_{env} term from the experimental band maximum position), and thus effectively (c) eliminates the above mentioned problem with the sensitivity of the vertical energy to the choice of geometry.

In our approach we choose COSMO, rather than vacuum geometries, as the former ones are usually closer to crystalline geometries,[11,72] and thus typically lead to smaller δ_{env} corrections. For example, in the case of **B3** considered before,[11] the δ_{env} correction to the singlet–triplet vertical excitation energy is only −0.6 kcal/mol with respect to the COSMO geometry (present choice), but would be −4.2 kcal/mol for the vacuum geometry. The effect is even more pronounced for $[Fe(CN)_6]^{4-}$ (**B2**), in which the δ_{env} correction for the singlet–triplet vertical excitation energy would be greater than 20 kcal/mol with respect to the vacuum geometry, to be compared with only

−3.5 kcal/mol with respect to the COSMO geometry (Table S11, Supporting Information). The difference is related mainly to the Fe-C distance being much longer in vacuum (1.986 Å) than in the crystal (1.918 Å) or COSMO model (1.912 Å). Similar differences between the gaseous and crystalline geometries of TM cyanides were noticed by Hocking et al.[127] Interestingly, even in the case of $K_4[Fe(CN)_6]\cdot 3H_2O$ where strong $CN^-\cdots K^+$ bonding interactions[128] are present in the crystal structure (and in our cluster model), it is mainly the geometry of the inner $[Fe(CN)_6]^{4-}$ that determines the δ_{env} correction; the interactions with added K^+ cations and the rest of ionic lattice contribute only 0.5 kcal/mol (cf Table S11).

As mentioned above, all the experimental data of complexes **B1**–**B4** and **C1**–**C4** were obtained for solid-state compounds with known crystal structures (see references below Table 1) and diffuse reflectance spectroscopy was used to record their spin-forbidden d–d transitions in solid state. The reflectance spectra of complexes **B1**–**B4** and **C1**–**C4** are provided in Figures S1–S8, Supporting Information. These are new experimental data with the exception of $K_3[Fe(CN)_6]$ (containing **B1**), for which we used a good quality reflectance spectrum available in the literature.[108] For $K_3[Fe(ox)_3]\cdot 3H_2O$ (containing **C2**), the presently obtained spectrum is similar as given by Jorgensen[15] (fig. 8 therein), although his spectrum was provided in a very small size and without sufficient details, making it necessary to record the new one. The spin-forbidden bands of our interest are usually well resolved in these reflectance spectra, giving separate low-intensity maxima. Only in three cases (**B1**, **B2**, **C4**) they are overlapped on more intense spin–allowed bands, making it necessary to perform the Gaussian analysis for assigning the position of maximum.

Discussion of the Benchmark Set

Approximately one-half of the SSE17 set are SCO complexes with the energy differences (ΔE_{ad} values) from 3 to 7 kcal/mol. The rest of the SSE17 benchmark set is evenly divided into LS (**B1**–**B4**) or HS (**C1**–**C4**) non-SCO complexes, for which the reference spin–state splittings (ΔE_{ve} values) are much greater in magnitude. Due to the diversity of TMs, ligand-field strengths, and coordination architectures, the present SSE17 set is a significant step beyond the previous similar

attempts from our group, which were limited to four Fe octahedral complexes[63] or metallocenes.[64]

Compared with the set of octahedral complexes studied in ref 63, we now treat the vibrational and environmental corrections more consistently. We also decided to exclude two of the previously studied complexes in view of some controversies associated with them. The first of these complexes, $[Fe(H_2O)_6]^{3+}$, is presently excluded in view of recurring suggestions [53a] that its sextet–quartet band could originate from a hydrolysis product. (An an-dept analysis of $[Fe(H_2O)_6]^{3+}$, which disproves these suggestions, will be published separately.) The second complex, $[Fe(en)_3]^{3+}$, is excluded due to the lack of experimental crystal structure of a compound in which the doublet–quartet absorption band described in the literature[129] could be conclusively observed to fullfil the requirements of our present methodology. (The previous analysis in ref 63 was based on the computed crystal structure of $[Fe(en)_3]Cl_3$, which was based on the assumption[129] that it is isomorphic to $[Cr(en)_3]Cl_3$. Despite undertaken efforts, we were unable so far to resolve the crystal structure of tentative $[Fe(en)_3]Cl_3$.) The two removed complexes are replaced in the SSE17 set by other HS Fe^{III} (**C1**, **C2**) or LS Fe^{III} (**B1**) complexes, showing analogous spin-forbidden transitions.

We found it challenging to meet the requirement of having simultaneously a reflectance spectrum and a crystal structure of a compound containing **C3**, which epitomizes the important class of HS $Mn^{II}N_6$ complexes. These complexes tend to be unstable towards oxidation and hence are difficult to handle in synthesis and measurements, possibly explaining the scarcity of appropriate data in the literature. Although Jørgensen[130] reported **C3** in solution (stabilized with hydrazine) already in 1969, no crystals were obtained. In 2017, Manke with co-workers[131] characterized the crystal structure of $[Mn(en)_3](OAc)_2$, whereas Ren with co-workers,[132] who used KI to stablize Mn^{II} complex, obtained crystalline $[Mn(en)_3]I_2$. We have modified the latter method to synthesize the chloride salt of **C3**, $[Mn(en)_3]Cl_2 \cdot H_2O$ (**1**), for which we now provide both the reflectance spectrum (Figure S7) and the crystal structure (CCDC 2259710, Supporting Information).

An important element of the SSE17 benchmark set are environmental (δ_{env}) and vibrational (δ_{vibr}) corrections. As can be seen from Table 1, both types of corrections can reach up to

3 kcal/mol in magnitude. The vibrational corrections are uniformly negative (under the sign convention (5)), which is due to the lowering of the vibrational frequencies upon transition from the lower-spin to the higher-spin state. The environmental corrections vary for different systems and can be both positive or negative. In some cases one of these corrections is negligible or the two corrections, taken together, tend to cancel out, but neither of these holds true in general. Thus, δ_{env} and δ_{vibr} corrections are generally important and it seems that neither of them is possible to predict (or neglect) in advance without performing the appropriate calculations. For vibronic corrections of non-SCO complexes the approximation $\delta_{\mathrm{env}} \approx 0.9\Delta\mathrm{ZPE}$ holds to within 0.9 kcal/mol (cf Table S8), which may be useful in future studies to roughly estimate these corrections.

It should be stressed as a side remark that the δ_{env} corrections used in this work are defined with respect to the COSMO/PBE0-D3(BJ) geometries, the same ones as used in subsequent single-point WFT and DFT calculations. The use of COSMO geometries is different from the previous work[63] where vacum geometries where used. The difference is of limited importance for adiabatic energies in SCO complexes, but potentially very important for vertical energies[11] (see also examples above). In any case, the present benchmark set is valid only for single-point calculations on top of the provided (COSMO/PBE0-D3(BJ)) geometries. Any modification of these geometries would require re-determination of the reference values by recomputing the δ_{env} corrections.

Of particular attention are SCO complexes characterized simultaneously in different environments: both in solution and in the crystal (**A5**, **A7**) or in several solvents (**A1**, **A4**). In such cases, the energy differences back-corrected from different environments are slightly different, reflecting limited accuracy of the methods used to quantify the δ_{env} term. We use the mean of the back-corrected values to provide the most objective reference value, whereas deviations of individual back-corrected values from the mean provide a rough measure of the uncertainty due to imperfect description of the environmental effects. In the case of **A5** (which was already discussed in the recent perspective[11]), the reference values back-corrected from acetone solution and BF_4^--crystal are in a relatively good mutual agreement, corresponding to the mean value of 5.2 kcal/mol with only 0.4 kcal/mol deviations of the individual values from the mean. An even better agreement

is observed in the case of **A7**, for which the energies back-corrected from the crystal and solution are identical to within 0.1 kcal/mol. In the case of **A1**, the energies back-corrected from different solvents span the range of 2.3–3.6 kcal/mol. The observed spread shows that variation of the experimental ΔH value with solvent is not perfectly paralleled by the calculations. Still, however, these data allow to estimate the reference energy difference for **A1** as the mean value of 3.0 kcal/mol with maximum deviation of 0.7 kcal/mol. In the case of **A4**, the values back-corrected from different solvents fall between 4.3 and 4.9 kcal/mol (mean 4.7 kcal/mol), which is again a good mutual agreement. It is obviously not possible to apply similar procedures in all cases (due to the lack of experimental data), but these examples suggest that uncertainties associated with estimation of the δ_{env} term are likely within 1 kcal/mol.

Other sources of error in our reference values are related to the δ_{vibr} correction, the δ_{subst} correction (for **A6** and **A7**) and uncertainties of the experimental data (e.g., from the fitting procedure used to determine the ΔH value; associated with reading the maximum of position of a weak d–d band, especially when Gaussian analysis has to be used to resolve overlapping bands). Overall, our tentative, but conservative estimate of possible errors in the reference values is 1–3 kcal/mol. This means that errors of 1 kcal/mol are relatively likely, whereas errors beyond 3 kcal/mol are increasingly unlikely. The SSE17 reference data are thus certainly not appropriate to discuss individual deviations in a sub-kcal/mol range. However, anticipating the results discussed below, many of the calculated spin–state splittings show much larger deviations, which can be hardly blamed on uncertainties of the reference data.

Performance of Quantum Chemistry Methods

Armed with the present SSE17 benchmark, we are now able to quantify the accuracy of spin–state energetics predicted by various quantum chemistry methods. To this end, Figures 2 and 3 show the distributions of errors in the SSE17 spin–state splittings calculated using selected WFT and DFT methods, respectively. The signed errors being analyzed are deviations of the calculated values from the corresponding reference values (from Table 1). The distribution of errors is presented

is the form of box-plot, whereas the mean absolute error (MAE) of each method is shown as point-plot. Numeric data for individual complexes and additional error statistics can be found in Supporting Information (Tables S14 and S15).

WFT Methods

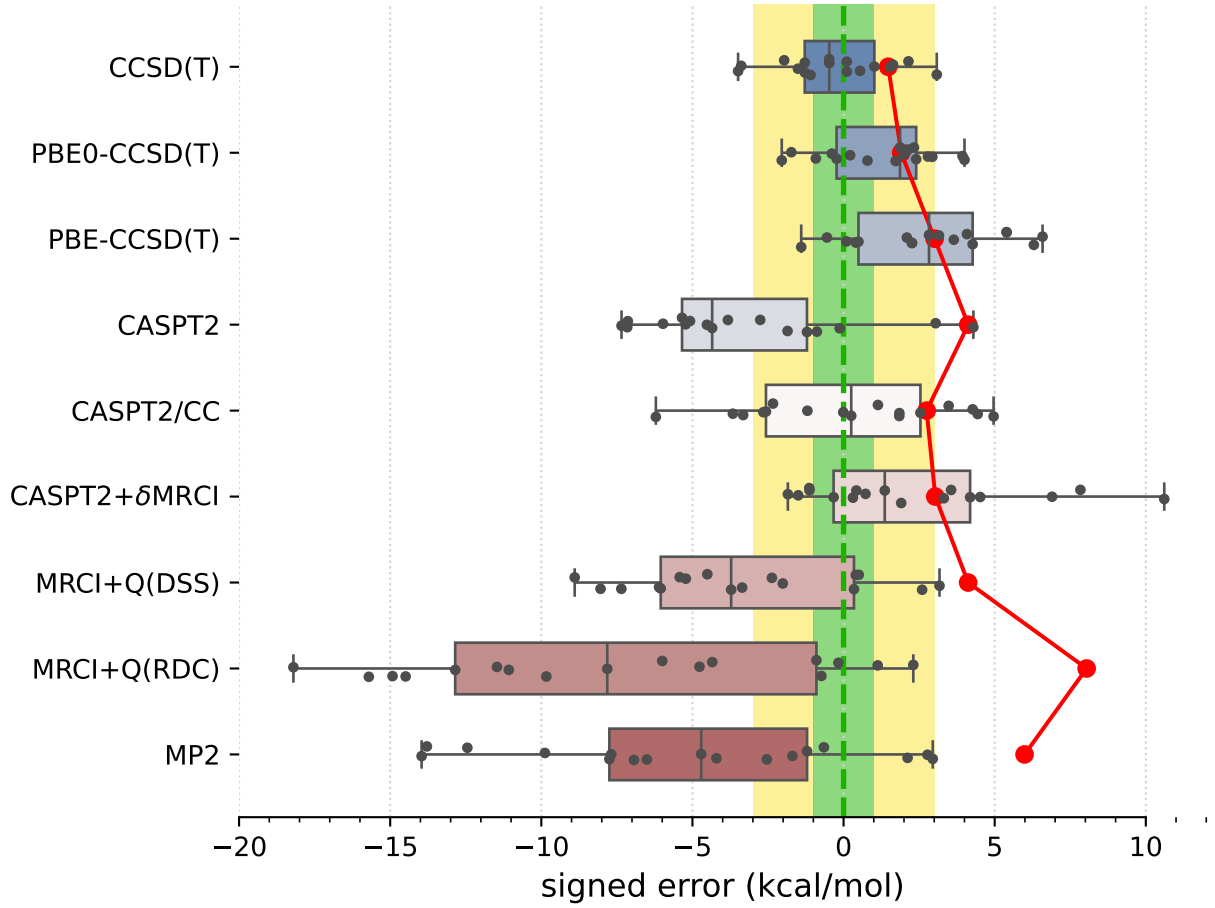

Figure 2: Distribution of errors in the SSE17 spin–state splittings calculated using selected WFT methods (box-plot) and the resulting MAE of each method (point-plot). Each box represents 50% of the population (with the median marked in the middle) and the whiskers extend from the minimum to the maximum of the population. Individual data are show as points. To guide the eye, error ranges ± 1 kcal/mol ("chemical accuracy") and ± 3 kcal/mol ("TM chemical accuracy") are colored in green and yellow, respectively.

We have benchmarked several WFT methods that were previously recommended for computation of spin–state energetics: CCSD(T) with HF reference orbitals and KS-CCSD(T) with either

PBE or PBE0 reference orbitals (i.e., PBE-CCSD(T), PBE0-CCSD(T)), CASPT2, CASPT2/CC,[52] CASPT2+δMRCI,[53] and MRCI+Q (using CW internally-contracted formulation[86]). We also included MP2 for comparison. Note that all WFT methods were applied without any local-correlation approximations and their results are approximate CBS limits (see Computational and Experimental Methods).

It is clear from Figure 2 than none of the benchmarked WFT methods can perfectly reproduce the reference data (which also have intrinsic errors, possibly 1–3 kcal/mol, as was discussed above). However, the CCSD(T) method based on HF orbitals is able to reproduce the reference data most accurately, with the MAE of only 1.5 kcal/mol, the RMSD (root mean square deviation) of 1.8 kcal/mol and the maximum error of -3.5 kcal/mol. The inspection of CCSD(T) results for individual complexes (Table S14) reveals that largest negative errors, indicative of the higher-spin state being overstabilized, are observed for Fe^{III} complexes **A1** and **B1**. The largest positive error, indicative of the lower-spin state being overstabilized, is observed for Co^{III} complex **B4**. The occurrences of positive and negative errors are well balanced across the SSE17 set, resulting in the mean and median errors within -0.5 kcal/mol. Thus, the CCSD(T) method appears to be (on average) not significantly biased toward either higher-spin or lower-spin states. We have also carefully investigated whether the observed small errors can be correlated with various diagnostics of multireference character, and the answer obtained is definitely negative (Supporting Information, section S4.2).

An interesting question, widely discussed in the literature,[45,48,133–136] is whether switching from HF to KS orbitals in the reference Slater determinant leads to more accurate CCSD(T) energetics. Looking at the present results, we can compare the accuracy of CCSD(T) energetics based on three choices of orbitals: HF, PBE0 (25% exact exchange), and PBE (no exact exchange). For some complexes, the use of PBE0 or PBE orbitals is beneficial to reduce the CCSD(T) errors (e.g., **A1**, **A7**), but for other cases the errors increase (e.g., **A3**–**A5**) or there is almost no effect (e.g., **A8**). Overall, the MAE and maximum error are greater for PBE-CCSD(T) and PBE0-CCSD(T) than for genuine CCSD(T). Thus, although some improvement may be observed for certain complexes, our

data give no support the hypothesis that the use of KS orbitals is systematically better than the use of HF orbitals. (In fact, the opposite is true for the presently studied SSE17 data, although the deterioration of the accuracy is minor.) These observations agree with the conclusions of Benedek et al.,[136] who also observed no systematic improvement in the CC energies of small molecules when switching from HF to KS orbitals.

Note that some of the recent claims advocating the usage of KS orbitals in CCSD(T) calculations[135,137] were based on the CCSD(T) energies calculated under the DLPNO (domain-based local-pair natural orbitals) approximation. The accuracy of this approximation may depend on the type of reference orbitals and sometimes strongly degrades when HF orbitals are used.[48,71] This probably explains the observed stronge dependence of spin–state energetics on the type of reference orbitals in the DLPNO-CCSD(T) studies as well as therein claimed significant improvement of the accuracy upon switching from HF to KS orbitals. However, these effects are specific to the DLPNO approximation and are not general features of the CCSD(T) method. In our study, which is based on canonical CCSD(T) method, i.e., without any local correlation approximations, the effect of switching from HF to KS orbitals is generally smaller than in the DLPNO-based studies (see also discussion in ref 71).

Relatively high accuracy of the CCSD(T) spin–state energetics has been already noted in our previous benchmark study of four Fe complexes.[63] In that work, the reduction of the CCSD(T)'s error by 1.6 kcal/mol by switching from HF to KS orbitals (B3LYP, 20% of exact exchange) was observed for one of the investigated complexes $[Fe(tacn)_2]^{2+}$, which is identical with the present **A4**. However, such improvement is no longer observed in the present study, which is due to the combination of reasons. First, the presently determined reference value for **A4** is higher by 0.9 kcal/mol than that determined in ref 63 due to the usage of different functional in determination of the δ-corrections and deriving the present reference value by averaging data back-corrected from three solvents. Second, the presently determined CCSD(T) energy is smaller than that in ref 63, which is mainly caused by the usage of more reliable[71] CCSD(T#)-F12a method to determine the CBS limit in the present work. Finally, we realized that in order to properly capture the (T) energy

term in KS-CCSD(T) calculations, one should use the open-shell CC program even for closed-shell singlets, which was not the case in ref 63. If the KS-(T) term is computed properly, the KS-CCSD(T) method leads to larger splitting than the CCSD(T) method (opposite to the behavior observed in ref 63). Consequently, not only for **A4**, but also for all other Fe^{II} SCO complexes included in the SSE17 set (**A2**–**A6**), HF-based CCSD(T) calculations yield smaller singlet–quintet gaps than either PBE0-CCSD(T) or PBE-CCSD(T).

Proceeding now to multireference methods, we observe the already known[52,63] tendency of the CASPT2 method (with the standard choice of active space and the default value of the IPEA shift parameter) to overstabilize higher-spin states, i.e., CASPT2 calculations usually lead to negative errors in the SSE17 benchmark, with the mean signed error of -3.3 kcal/mol, maximum error of -7.4 kcal/mol, and the MAE of 4.1 kcal/mol. The negative errors observed in CASPT2 calculations are reduced by both CASPT2/CC and CASPT2+δMRCI methods. For CASPT2/CC, the median and the mean signed error are very close to zero. For CASPT2+δMRCI, the mean signed error is about 2 kcal/mol. Both of these methods have MAE of ca. 3 kcal/mol. Somewhat surprisingly, however, for organometallic complexes **A8** and **A9**, the genuine CASPT2 method leads to positive errors of 3–4 kcal/mol, which neither CASPT2/CC nor CASPT2+δMRCI can reduce (cf Table S14). In fact, complex **A8** is responsible for the maximum error (nearly $+11$ kcal/mol) of the CASPT2+δMRCI method. Other considerable outliers for the CASPT2+δMRCI method are complexes **A2** and **A8**, with errors of 7–8 kcal/mol. In the case of CASPT2/CC, the largest error of -6 kcal/mol is observed for **A7**.

It has been suggested [53b] that the CASPT2+δMRCI method outperforms CCSD(T) for complexes with significant π-backdonation. However, this conjecture is not confirmed by the SSE17 benchmark, in which **A6**, **B1** and **B2** (with cyanide ligands) and **A8** and **A9** (with Cp ligands) are typical complexes featuring π-backdonation. Inspections of the detailed results (Table S14), reveals that for none of these complexes the CASPT2+δMRCI method is significantly more accurate than CCSD(T). In fact, we observe a slight improvement only for **B1** (CCSD(T) error of -3.4 kcal/mol, CASPT2+δMRCI error of -1.8 kcal/mol), but a slight deterioration for **B2**

(CCSD(T) error of 0.5 kcal/mol, CASPT2+δMRCI error of 4.2 kcal/mol) and a significant deterioration for **A8** and **A9**, for which CASPT2+δMRCI has errors of 10.6 and 7.8 kcal/mol, respectively.

Although CASPT2+δMRCI was originally motivated as a computationally tractable approximation to more expensive MRCI [53a], our data shows that it is actually more accurate than MRCI+Q itself. This is presumably due to the size-consistency problem in truncated MRCI, which is only partially resolved by adding an approximate size-consistency correction in the MRCI+Q approach. This problem is alleviated in the CASPT2+δMRCI method, where only a small numer of active electrons plus 8 electrons on TM 3s3p orbitals undergo the MRCI treatment.[53] In our MRCI+Q calculations (in which all valence and TM 3s3p electrons were correlated), we compared several size-consistency corrections:[138] the original Davidson correction (DC), the renormalized DC (RDC), the Davidson–Silver–Siegbahn (DSS) correction, and the Pople correction (PC). Only the DSS and RDC results are presented in Figure 2, but all can be found in Table S14, Supporting Information. For the present set of spin–state energetics, the most accurate formulation is MRCI+Q(DSS), which has statistical errors similar as CASPT2, closely followed by the MRCI+Q(PC), whereas MRCI+Q(RDC) and MRCI+Q(DC) lead to much larger errors, which are in fact greater than MP2 errors. Inspection of the detailed results (Table S14) reveals that discrepancies between different size-consistency corrections are more pronounced for larger complexes, i.e., with a greater number of correlated electrons, suggesting these errors are connected with the violation of size-consistency. The analogous problems of MRCI+Q calculations were also observed in our previous study of four complexes,[63] and are now fully confirmed for the larger SSE17 set.

DFT Methods.

We have benchmarked 32 functionals from different rungs of the Jacob's ladder: gradient functionals (PBE, OLYP, OPBE, SSB, S12g, B97), meta-gradient functionals (TPSSh, M06L, MN15L, MVS, SCAN, R2SCAN), global hybrids (PBE0, B3LYP, B3LYP*, S12h) and meta-hybrids (TPSSh, M06, MN15, PW6B95, MVSh), range-separated hybrids (CAM-B3LYP, LC-ωPBE, ωB97X-

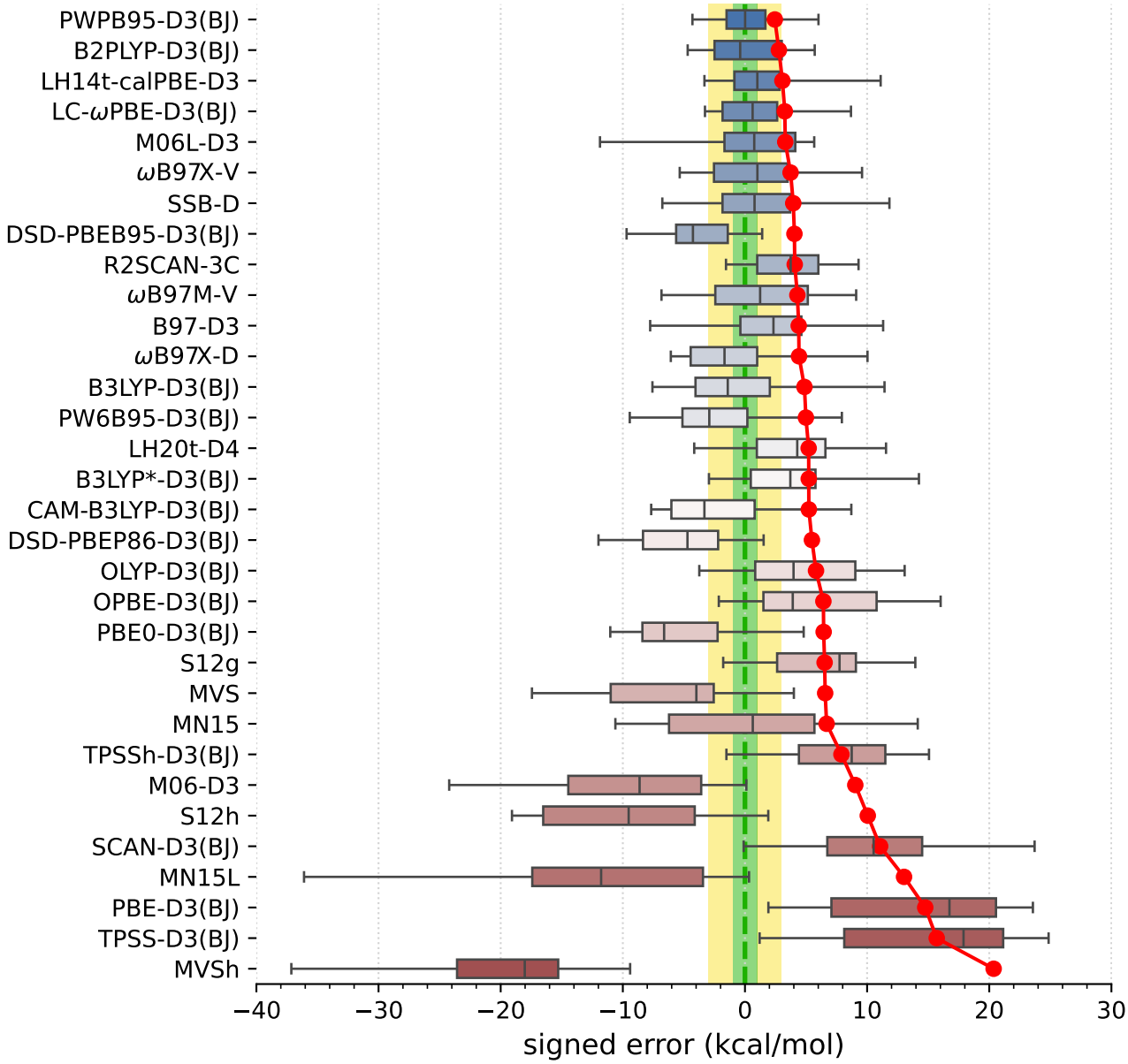

Figure 3: Distribution of errors in the SSE17 spin–state splittings calculated using selected DFT methods (box-plot) and the resulting MAE of each method (point-plot).

V/D, ωB97M-V), local-hybrids (LH14t-calPBE, LH20t), and double-hybrids (PWPB95, B2PLYP, DSD-PBEB95, DSD-PBEP86); see Supporting Information for references. Most functionals were benchmarked with appropriate dispersion corrections.

In view of the results shown in Figure 3 (for corresponding numeric data, see Table S15, Supporting Information), the best performers are double-hybrid functionals PWPB86-D3(BJ) and B2PLYP-D3(BJ). These two functionals show relatively small MAEs (2.4 and 2.8 kcal/mol, respectively), nearly zero mean signed and median errors, and maximum errors within 6 kcal/mol. The other two tested double-hybrids (DSD-PBEB95/PBEP86-D3(BJ)) perform considerably worse, showing overstabilization of higher-spin states. Some other functionals highly ranked in the SSE17 benchmark are the following: local hybrid LH14t-calPBE-D3(BJ),[139] range-separated hybrid LC-ωPBE-D3(BJ),[140] meta-gradient M06L-D3,[141] range separated meta-hybrid with nonlocal dispersion ωB87X-V,[142] and gradient functional SSB-D.[143] All these have MAEs within 4 kcal/mol, and mean signed errors within 2 kcal/mol, but all of them also feature maximum errors of about 9 kcal/mol or greater.

Functionals traditionally recommended for spin states of TM complexes,[29,65,144,145] such as B3LYP*-D3(BJ) and TPSSh-D3(BJ) hybrids with 10–15 % of exact exchange, do not perform well in the SSE17 benchmark. These two functionals have MAE of 4.3 and 7.7 kcal/mol, respectively, and lead to maximum errors of 14–15 kcal/mol. Inspection of numeric results (cf Table S15) reveals that these maximum errors are due to overstabilization of lower-spin states in HS complexes **C1**–**C4**, but even if we restrict our attention to SCO complexes **A1**–**A8** (or even narrower class of Fe^{II} SCO complexes **A2**–**A6**), these two functionals are also by no means optimal. In fact, uncorrected B3LYP-D3(BJ) with 25% of exact exchange is globally a better performer than B3LYP*-D3(BJ). When restricted to SCO complexes, B3LYP* is better than B3LYP, providing e.g. accurate results for **A1**, **A4**, and **A9**, but it leads to significant errors of 4–6 kcal/mol for **A2**, **A3**, **A6** and **A7**. The inferior performance of B3LYP* and TPSSh functionals, particularly their significant overstabilization of the quartet state with respect to sextet state in complexes **C1**–**C3**, agrees with similar problems of these functionals evidenced in a different benchmark SSCIP6,

which is based on probing the ability to reproduce correct ground states in the set of crystalline iron-porphyrins.[120]

The lack of universality is a problem of many approximate DFT methods. To illustrate this point, Figure 4 present mean signed errors of selected methods separately for SCO (**A1**–**A9**) and non-SCO (**B1**–**B4**, **C1**–**C4**) complexes, and for the entire SSE17 set. With CCSD(T) and CASPT2/CC wave-function methods, the errors observed for different classes are comparable, and similar behavior is also found for PWPB95-D3(BJ) double hybrid functional. The TPSSh-D3(BJ) and MVS are examples of functionals giving rather universally positive or negative errors. By contrast, LH14t-calPBE-D3 is very accurate for SCO complexes, but features significant positive errors for non-SCO complexes. Comparable non-universal behavior is observed for B3LYP-D3(BJ), B3LYP*-D3(BJ) and to some extent even for B2PLYP-D3(BJ).

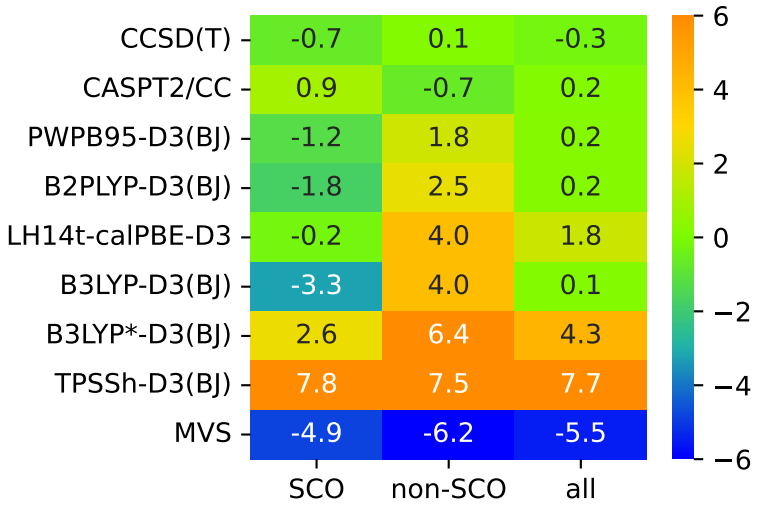

Figure 4: Mean signed errors (kcal/mol) of selected methods for different classes of complexes.

Conclusions

Adhering to recently recommended strategy of developing benchmark sets for theory in close cooperation with experiment,[146] we have presented the novel benchmark set for first-row TM spin–state energetics (SSE17), which is based on curated experimental data of 17 chemically diverse com-

plexes, classical and organometallic ones, containing various metals and having different ligand-field strengths. The employed experimental data, which are SCO enthalpies or spin-forbidden d–d excitation energies, originate in condensed-phase measurements, but are suitably back-corrected for environmental and vibrational effects to produce reference data directly comparable to electronic energy differences of isolated complexes in vacuum. The presented benchmark set is not only useful for assessing the accuracy of existing quantum chemistry methods, but it is also hoped to be useful for validation of new methods, parameterization of new functionals or developing machine-learning models.

This is the first time that performance of both WFT and DFT quantum chemistry method can be quantitatively benchmarked against such an extensive and statistically relevant set of experiment-derived spin–state energetics. The results of benchmarking confirm a high accuracy of the single-reference CCSD(T) method, which across the SSE17 set features the mean absolute error (MAE) of 1.5 kcal/mol, the mean signed error of –0.3 kcal/mol, and the maximum error of 3.5 kcal/mol. Contrary to earlier claims, we have found that the overall accuracy of CCSD(T) spin–state energetics does not systematically improve by using KS orbitals (PBE or PBE0) instead of HF orbitals. The deviations of CCSD(T) spin–state energetic from the benchmark values do not seem to be correlated with any common diagnostic of multireference character. Among several multireference approaches that have been benchmarked, the variational MRCI+Q method does not appear to outperform computationally much cheaper CASPT2; both of them produce MAE of 4 kcal/mol and maximum errors of around 7–9 kcal/mol. The form of size-consistency correction is critically important for the accuracy of MRCI+Q. The recently proposed methods CASPT2/CC and CASPT2+δMRCI outperform the original CASPT2 method in terms of typical errors (MAE values of around 3 kcal/mol), but they still lead to considerable maximum errors for some outliers. Neither of the tested multireference methods can consistently outperform the single-reference CCSD(T) method across the SSE17 set. Among 32 approximate DFT methods that have been benchmarked, the best performers are double-hybrids (PWPB95-D3(BJ) and B2PLYP-D3(BJ)), which due to the MAEs within 3 kcal/mol, the mean signed errors of only 0.2 kcal/mol, and the maximum errors

within 6 kcal/mol appear to be (on average) equally accurate as CASPT2/CC. Our results confirm that the non-universality problem exist in many approximate DFT methods. The functionals traditionally recommended for spin–state energetics, such as TPSSh-D3(BJ) or B3LYP*-D3(BJ) and containing 10–15 % of exact exchange, do not perform well across the SSE17 benchmark by yielding the MAEs of, respectively, 5 or 8 kcal/mol and maximum errors beyond 10 kcal/mol. One should be aware of such problems in computational reactivity studies, where these or similar hybrid functionals are still predominantly used. A practical solution for DFT-based reactivity studies is, for example, to add relatively simple corrections based on CCSD(T) spin–state energetics of simplified models.[33]

Acknowledgement

This research was supported by National Science Centre, Poland, under grant no. 2017/26/D/ST4/00774. We gratefully acknowledge Polish high-performance computing infrastructure PLGrid (HPC Centers: ACK Cyfronet AGH, PCSS) for providing computer facilities and support within computational grants no. PLG/2024/016907, PLG/2023/016069 and PLG/2022/015281. The study was partially carried out using research infrastructure purchased with the funds of the European Union in the framework of the Smart Growth Operational Programme, Measure 4.2; Grant No. POIR.04.02.00-00-D001/20, "ATOMIN 2.0 - ATOMic scale science for the INnovative economy."

Supporting Information Available

Reflectance spectra evidencing spin-forbidden d–d absorption bands, details of crystal structure determination for $[Mn(en)_3]Cl_2 \cdot H_2O$, full computational details, details of calculating the vibrational environmental and substituent corrections, tabulation of all WFT and DFT results used to prepare Figures 2 and 3 (PDF); optimized Cartesian coordinates for complexes comprising the SSE17 benchmark set (TXT); total energies and $\langle S^2 \rangle$ values (XLSX); crystalographic information file for $[Mn(en)_3]Cl_2 \cdot H_2O$ (CIF). Additional supporting data (structures and total energies

from selected calculations) may be accessed as an ioChem-BD collection under the following link: `https://doi.org/10.19061/iochem-bd-7-8`.

References

(1) Swart, M., Costas, M., Eds. *Spin States in Bioinorganic and Inorganic Chemistry: Influence on Structure and Reactivity*; Wiley, 2015.

(2) Blomberg, M. R. A.; Borowski, T.; Himo, F.; Liao, R.-Z.; Siegbahn, P. E. M. Quantum Chemical Studies of Mechanisms for Metalloenzymes. *Chem. Rev.* **2014**, *114*, 3601–3658.

(3) Nandy, A.; Duan, C.; Taylor, M. G.; Liu, F.; Steeves, A. H.; Kulik, H. J. Computational Discovery of Transition-metal Complexes: From High-throughput Screening to Machine Learning. *Chem. Rev.* **2021**, *121*, 9927–10000.

(4) Mancuso, J. L.; Mroz, A. M.; Le, K. N.; Hendon, C. H. Electronic Structure Modeling of Metal-Organic Frameworks. *Chem. Rev.* **2020**, *120*, 8641–8715.

(5) Bols, M. L.; Rhoda, H. M.; Snyder, B. E. R.; Solomon, E. I.; Pierloot, K.; Schoonheydt, R. A.; Sels, B. F. Advances in the synthesis, characterisation, and mechanistic understanding of active sites in Fe-zeolites for redox catalysts. *Dalton Trans.* **2020**, *49*, 14749–14757.

(6) Vogiatzis, K. D.; Polynski, M. V.; Kirkland, J. K.; Townsend, J.; Hashemi, A.; Liu, C.; Pidko, E. A. Computational Approach to Molecular Catalysis by 3d Transition Metals: Challenges and Opportunities. *Chem. Rev.* **2019**, *119*, 2453–2523.

(7) Swart, M. *New Directions in the Modeling of Organometallic Reactions*; Topics in Organometallic Chemistry; Springer: Cham, 2020; Vol. 67; pp 191–226.

(8) Swart, M. Spin States of (Bio)inorganic Systems: Successes and Pitfalls. *Int. J. Quantum Chem.* **2013**, *113*, 2–7.

(9) Harvey, J. N. On the accuracy of density functional theory in transition metal chemistry. *Annu. Rep. Prog. Chem., Sect. C: Phys. Chem.* **2006**, *102*, 203–226.

(10) Feldt, M.; Phung, Q. M. Ab Initio Methods in First-Row Transition Metal Chemistry. *Eur. J. Inorg. Chem.* **2022**, e202200014.

(11) Radoń, M. Benchmarks for transiton metal spin–state energetics: Why and how to employ experimental reference data? *Phys. Chem. Chem. Phys.* **2023**, *25*, 30800–30820.

(12) Kepp, K. P. In *Transition Metals in Coordination Environments: Computational Chemistry and Catalysis Viewpoints*; Broclawik, E., Borowski, T., Radoń, M., Eds.; Challenges and Advances in Computational Chemistry and Physics; Springer International Publishing: Cham, 2019; Vol. 29; Chapter 1, pp 1–33.

(13) Gütlich, P., Goodwin, H., Eds. *Spin Crossover in Transition Metal Compounds I*; Springer, 2004.

(14) Halcrow, M. A., Ed. *Spin-Crossover Materials*; Wiley, 2013.

(15) Jørgensen, C. K. *Absorption Spectra and Chemical Bonding in Complexes*; Pergamon Press, 1962.

(16) Srnec, M.; Wong, S. D.; England, J.; Que, L.; Solomon, E. I. π-Frontier molecular orbitals in S = 2 ferryl species and elucidation of their contributions to reactivity. *Proc. Natl. Acad. Sci.* **2012**, *109*, 14326–14331.

(17) Rice, D. B.; Wong, D.; Weyhermüller, T.; Neese, F.; DeBeer, S. The spin-forbidden transition in iron(IV)-oxo catalysts relevant to two-state reactivity. *Science Advances* **2024**, *10*, eado1603.

(18) (a) Poli, R.; Harvey, J. N. Spin Forbidden Chemical Reactions of Transition Metal Compounds. New Ideas and New Computational Challenges. *Chem. Soc. Rev.* **2003**, *32*, 1–8; (b) Harvey, J. N.; Poli, R.; Smith, K. M. Understanding the reactivity of transition metal

complexes involving multiple spin states. *Coord. Chem. Rev.* **2003**, *238-239*, 347–361; (c) Harvey, J. N. Spin-forbidden reactions: computational insight into mechanisms and kinetics. *WIREs Comput. Mol. Sci.* **2014**, *4*, 1–14.

(19) Schröder, D.; Shaik, S.; Schwarz, H. Two-State Reactivity as a New Concept in Organometallic Chemistry. *Acc. Chem. Res.* **2000**, *33*, 139–145.

(20) (a) Shaik, S.; Chen, H.; Janardanan, D. Exchange-Enhanced Reactivity in Bond Activation by Metal–Oxo enzymes and Synthetic Reagents. *Nature Chemistry* **2011**, *3*, 19–27; (b) Wang, B.; Wu, P.; Shaik, S. Critical Roles of Exchange and Superexchange Interactions in Dictating Electron Transfer and Reactivity in Metalloenzymes. *J. Phys. Chem. Lett.* **2022**, *13*, 2871–2877.

(21) Kepp, K. P. Heme: From quantum spin crossover to oxygen manager of life. *Coord. Chem. Rev.* **2017**, *344*, 363–374.

(22) Lábas, A.; Menyhárd, D. K.; Harvey, J. N.; Oláh, J. First Principles Calculation of the Reaction Rates for Ligand Binding to Myoglobin: The Cases of NO and CO. *Chem. Eur. J.* **2018**, *24*, 5350–5358.

(23) Swart, M. Accurate Spin-State Energies for Iron Complexes. *J. Chem. Theory Comput.* **2008**, *4*, 2057–2066.

(24) Radoń, M.; Srebro, M.; Broclawik, E. Conformational Stability and Spin States of Cobalt(II) Acetylacetonate: CASPT2 and DFT Study. *J. Chem. Theory Comput.* **2009**, *5*, 1237–1244.

(25) Phung, Q. M.; Nam, H. N.; Saitow, M. Unraveling the Spin-State Energetics of FeN_4 Complexes with Ab Initio Methods. *J. Phys. Chem. A* **2023**, *127*, 7544–7556.

(26) (a) Blomberg, M. R. A.; Siegbahn, P. E. M. How cytochrome c oxidase can pump four protons per oxygen molecule at high electrochemical gradient. *BBA - Bioenergetics* **2015**,

1847, 364–376; (b) Blomberg, M. R. A. Mechanism of Oxygen Reduction in Cytochrome c Oxidase and the Role of the Active Site Tyrosine. *Biochemistry* **2016**, *55*, 489–500.

(27) Cho, Y.; Laplaza, R.; Vela, S.; Corminboeuf, C. Automated prediction of ground state spin for transition metal complexes. *Digital Discovery* **2024**, Advance article, DOI: 10.1039/D4DD00093E.

(28) Hehn, L.; Deglmann, P.; Kühn, M. Chelate Complexes of 3d Transition Metal Ions—A Challenge for Electronic-Structure Methods? *J. Chem. Theory Comput.* **2024**, *20*, 4545–4568.

(29) Kepp, K. P. Theoretical Study of Spin Crossover in 30 Iron Complexes. *Inorg. Chem.* **2016**, *55*, 2717–2727.

(30) Cirera, J.; Via-Nadal, M.; Ruiz, E. Benchmarking Density Functional Methods for Calculation of State Energies of First Row Spin-Crossover Molecules. *Inorg. Chem.* **2018**, *57*, 14097–14105.

(31) Cirera, J.; Ruiz, E. Computational Modeling of Transition Temperatures in Spin-Crossover Systems. *Comments Inorg. Chem.* **2019**, *39*, 216–241.

(32) Vennelakanti, V.; Kilic, I. B.; Terrones, G. G.; Duan, C.; Kulik, H. J. Machine Learning Prediction of the Experimental Transition Temperature of Fe(II) Spin-Crossover Complexes. *J. Phys. Chem. A* **2024**, *128*, 204–216.

(33) Oszajca, M.; Drabik, G.; Radoń, M.; Franke, A.; van Eldik, R.; Stochel, G. Experimental and Computational Insight into the Mechanism of NO Binding to Ferric Microperoxidase. The Likely Role of Tautomerization to Account for the pH Dependence. *Inorg. Chem.* **2021**, *60*, 15948–15967.

(34) Radoń, M.; Gąssowska, K.; Szklarzewicz, J.; Broclawik, E. Spin-State Energetics of Fe(III)

and Ru(III) Aqua Complexes: Accurate ab Initio Calculations and Evidence for Huge Solvation Effects. *J. Chem. Theory Comput.* **2016**, *12*, 1592–1605.

(35) Radoń, M.; Drabik, G. Spin States and Other Ligand–Field States of Aqua Complexes Revisited with Multireference Methods Including Solvation Effects. *J. Chem. Theory Comput.* **2018**, *14*, 4010–4027.

(36) Stavretis, S. E.; Atanasov, M.; Podlesnyak, A. A.; Hunter, S. C.; Neese, F.; Xue, Z.-L. Magnetic Transitions in Iron Porphyrin Halides by Inelastic Neutron Scattering and Ab Initio Studies of Zero-Field Splittings. *Inorg. Chem.* **2015**, *54*, 9790–9801.

(37) Sauza-de la Vega, A.; Pandharkar, R.; Stroscio, G. D.; Sarkar, A.; Truhlar, D. G.; Gagliardi, L. Multiconfiguration Pair-Density Functional Theory for Chromium(IV) Molecular Qubits. *JACS Au* **2022**, *2*, 2029–2037.

(38) Radoń, M. Role of Spin States in Nitric Oxide Binding to Cobalt(II) and Manganese(II) Porphyrins. Is Tighter Binding Always Stronger? *Inorg. Chem.* **2015**, *54*, 5634–5645.

(39) Reiher, M.; Salomon, O.; Hess, B. A. Reparameterization of hybrid functionals based on energy differences of states of different multiplicity. *Theor. Chem. Acc.* **2001**, *107*, 48–55.

(40) Aoki, Y. et al. Physical methods for mechanistic understanding: general discussion. *Faraday Discuss.* **2019**, *220*, 144–178.

(41) Fumanal, M.; Wagner, L. K.; Sanvito, S.; Droghetti, A. Diffusion Monte Carlo Perspective on the Spin-State Energetics of $[Fe(NCH)_6]^{2+}$. *J. Chem. Theory Comput.* **2016**, *12*, 4233–4241.

(42) Song, S.; Kim, M.-C.; Sim, E.; Benali, A.; Heinonen, O.; Burke, K. Benchmarks and Reliable DFT Results for Spin Gaps of Small Ligand Fe(II) Complexes. *J. Chem. Theory Comput.* **2018**, *14*, 2304–2311.

(43) Lawson Daku, L. M.; Aquilante, F.; Robinson, T. W.; Hauser, A. Accurate Spin-State Energetics of Transition Metal Complexes. 1. CCSD(T), CASPT2, and DFT Study of $[M(NCH)_6]^{2+}$ (M = Fe, Co). *J. Chem. Theory Comput.* **2012**, *8*, 4216–4231.

(44) Flöser, B. M.; Guo, Y.; Riplinger, C.; Tuczek, F.; Neese, F. Detailed Pair Natural Orbital-based Coupled Cluster Studies of Spin Crossover Energetics. *J. Chem. Theory Comput.* **2020**, *16*, 2224–2235.

(45) Harvey, J. N.; Aschi, M. Modelling spin-forbidden reactions: recombination of carbon monoxide with iron tetracarbonyl. *Faraday Discuss.* **2003**, *124*, 129–143.

(46) Olah, J.; Harvey, J. NO Bonding to Heme Groups: DFT and Correlated Ab Initio Calculations. *J. Phys. Chem. A* **2009**, *113*, 7338–7345.

(47) Radoń, M. Spin-State Energetics of Heme-Related Models from DFT and Coupled Cluster Calculations. *J. Chem. Theory Comput.* **2014**, *10*, 2306–2321.

(48) Drosou, M.; Mitsopoulou, C. A.; Pantazis, D. A. Reconciling Local Coupled Cluster with Multireference Approaches for Transition Metal Spin-State Energetics. *J. Chem. Theory Comput.* **2022**, *18*, 3538–3548.

(49) Römer, A.; Hasecke, L.; Blöchl, P.; Mata, R. A. A Review of Density Functional Models for the Description of Fe(II) Spin-Crossover Complexes. *Molecules* **2020**, *25*, 5176.

(50) Stein, C. J.; von Burg, V.; Reiher, M. The Delicate Balance of Static and Dynamic Electron Correlation. *J. Chem. Theory Comput.* **2016**, *12*, 3764–3773.

(51) (a) Pierloot, K.; Vancoillie, S. Relative Energy of the High-($^5T_{2g}$) and Low-($^1A_{1g}$) Spin States of $[Fe(H2O)_6]^{2+}$, $[Fe(NH_3)_6]^{2+}$, and $[Fe(bpy)_3]^{2+}$: CASPT2 versus Density Functional Theory. *J. Chem. Phys.* **2006**, *125*, 124303; (b) Pierloot, K.; Vancoillie, S. Relative energy of the high-($^5T_{2g}$) and low-($^1A_{1g}$) spin states of the ferrous complexes $[Fe(L)(NHS_4)]$: CASPT2 versus density functional theory. *J. Chem. Phys.* **2008**, *128*, 034104.

(52) Phung, Q. M.; Feldt, M.; Harvey, J. N.; Pierloot, K. Towards Highly Accurate Spin State Energetics in First-Row Transition Metal Complexes: A Combined CASPT2/CC Approach. *J. Chem. Theory Comput.* **2018**, *14*, 2446–2455.

(53) (a) Reimann, M.; Kaupp, M. Spin-State Splittings in 3d Transition-Metal Complexes Revisited: Toward a Reliable Theory Benchmark. *J. Chem. Theory Comput.* **2023**, *19*, 97–108; (b) Reimann, M.; Kaupp, M. Spin-State Splittings in 3d Transition-Metal Complexes Revisited: Benchmarking Approximate Methods for Adiabatic Spin-State Energy Differences in Fe(II) Complexes. *J. Chem. Theory Comput.* **2022**, *28*, 7442–7456.

(54) Zhang, D.; Truhlar, D. G. Spin Splitting Energy of Transition Metals: A New, More Affordable Wave Function Benchmark Method and Its Use to Test Density Functional Theory. *J. Chem. Theory Comput.* **2020**, *16*, 4416–4428.

(55) Saitow, M.; Kurashige, Y.; Yanai, T. Fully Internally Contracted Multireference Configuration Interaction Theory Using Density Matrix Renormalization Group: A Reduced-Scaling Implementation Derived by Computer-Aided Tensor Factorization. *J. Chem. Theory Comput.* **2015**, *11*, 5120–5131.

(56) Wilbraham, L.; Verma, P.; Truhlar, D. G.; Gagliardi, L.; Ciofini, I. Multiconfiguration Pair-Density Functional Theory Predicts Spin-State Ordering in Iron Complexes with the Same Accuracy as Complete Active Space Second-Order Perturbation Theory at a Significantly Reduced Computational Cost. *J. Phys. Chem. Lett.* **2017**, *8*, 2026–2030.

(57) Stoneburner, S. J.; Truhlar, D. G.; Gagliardi, L. Transition Metal Spin-State Energetics by MC-PDFT with High Local Exchange. *J. Phys. Chem. A* **2020**, *124*, 1187–1195.

(58) Marti, K. H.; Ondík, I. M.; Moritz, G.; Reiher, M. Density matrix renormalization group calculations on relative energies of transition metal complexes and clusters. *J. Chem. Phys.* **2008**, *128*, 014104.

(59) Roemelt, M.; Pantazis, D. A. Multireference Approaches to Spin-State Energetics of Transition Metal Complexes Utilizing the Density Matrix Renormalization Group. *Adv. Theory Simul.* **2019**, *2*, 1800201.

(60) Li Manni, G.; Smart, S. D.; Alavi, A. Combining the Complete Active Space Self-Consistent Field Method and the Full Configuration Interaction Quantum Monte Carlo within a Super-CI Framework, with Application to Challenging Metal-Porphyrins. *J. Chem. Theory Comput.* **2016**, *12*, 1245–1258.

(61) Vitale, E.; Li Manni, G.; Alavi, A.; Kats, D. FCIQMC-Tailored Distinguishable Cluster Approach: Open-Shell Systems. *J. Chem. Theory Comput.* **2022**, *18*, 3427–3437.

(62) Neugebauer, H.; Vuong, H. T.; Weber, J. L.; Friesner, R. A.; Shee, J.; Hansen, A. Toward Benchmark-Quality Ab Initio Predictions for 3d Transition Metal Electrocatalysts: A Comparison of CCSD(T) and ph-AFQMC. *J. Chem. Theory Comput.* **2023**,

(63) Radoń, M. Benchmarking quantum chemistry methods for spin-state energetics of iron complexes against quantitative experimental data. *Phys. Chem. Chem. Phys.* **2019**, *21*, 4854–4870.

(64) Drabik, G.; Szklarzewicz, J.; Radoń, M. Spin–state energetics of metallocenes: How do best wave function and density functional theory results compare with the experimental data? *Phys. Chem. Chem. Phys.* **2021**, *23*, 151–172.

(65) Jensen, K. P.; Cirera, J. Accurate Computed Enthalpies of Spin Crossover in Iron and Cobalt Complexes. *J. Phys. Chem. A* **2009**, *113*, 10033–10039.

(66) Gómez-Coca, S.; Ruiz, E. Benchmarking Periodic Density Functional Theory Calculations for Spin-State Energies in Spin-Crossover Systems. *Inorg. Chem.* **2024**,

(67) Vela, S.; Fumanal, M.; Cirera, J.; Ribas-Arino, J. Thermal spin crossover in Fe(II) and

Fe(III). Accurate spin state energetics at the solid state. *Phys. Chem. Chem. Phys.* **2020**, *22*, 4938–4945.

(68) Ohlrich, M.; Powell, B. J. Fast, accurate enthalpy differences in spin crossover crystals from DFT+U. *J. Chem. Phys.* **2020**, *153*, 104107.

(69) Mariano, L. A.; Vlaisavljevich, B.; Poloni, R. Improved Spin-State Energy Differences of Fe(II) Molecular and Crystalline Complexes via the Hubbard U-Corrected Density. *J. Chem. Theory Comput.* **2021**, *17*, 2807–2816.

(70) Hughes, T. F.; Friesner, R. A. Correcting Systematic Errors in DFT Spin-Splitting Energetics for Transition Metal Complexes. *J. Chem. Theory Comput.* **2011**, *7*, 19–32.

(71) Drabik, G.; Radoń, M. Approaching the Complete Basis Set Limit for Spin–State Energetics of Mononuclear First-Row Transition Metal Complexes. *J. Chem. Theory Comput.* **2024**, *20*, 3199–3217.

(72) Hocking, R. K.; Deeth, R. J.; Hambley, T. W. DFT Study of the Systematic Variations in Metal-Ligand Bond Lengths of Coordination Complexes: the Crucial Role of the Condensed Phase. *Inorg. Chem.* **2007**, *46*, 8238–8244.

(73) Kortüm, G. *Reflectance Spectroscopy Principles, Methods, Applications*; Springer-Verlag: New York, 1969.

(74) Adamo, C.; Barone, V. Toward reliable density functional methods without adjustable parameters: The PBE0 model. *J. Chem. Phys.* **1999**, *110*, 6158–6170.

(75) Grimme, S.; Ehrlich, S.; Goerigk, L. Effect of the damping function in dispersion corrected density functional theory. *J. Comp. Chem.* **2011**, *32*, 1456–1465.

(76) Weigend, F.; Ahlrichs, R. Balanced basis sets of split valence, triple zeta valence and quadruple zeta valence quality for H to Rn: Design and assessment of accuracy. *Phys. Chem. Chem. Phys.* **2005**, *7*, 3297–3305.

(77) Klamt, A.; Schürmann, G. COSMO: a new approach to dielectric screening in solvents with explicit expressions for the screening energy and its gradient. *J. Chem Soc, Perkin Trans. 2* **1993**, 799.

(78) TURBOMOLE V7.5.1 2021, a development of University of Karlsruhe and Forschungszentrum Karlsruhe GmbH, 1989-2007, TURBOMOLE GmbH, since 2007; available from `https://www.turbomole.org`.

(79) Balasubramani, S. G. et al. TURBOMOLE: Modular program suite for ab initio quantum-chemical and condensed-matter simulations. *J. Chem. Phys.* **2020**, *152*, 184107.

(80) (a) Douglas, M.; Kroll, N. M. Quantum electrodynamical corrections to the fine structure of helium. *Ann. Phys.* **1974**, *82*, 89–155; (b) Hess, B. A. Relativistic electronic-structure calculations employing a two-component no-pair formalism with external-field projection operators. *Phys. Rev. A* **1986**, *33*, 3742–3748.

(81) Frisch, M. J. et al. Gaussian 16 Revision C.01. 2016; Gaussian Inc. Wallingford CT.

(82) Neese, F.; Wennmohs, F.; Becker, U.; Riplinger, C. The ORCA quantum chemistry program package. *J. Chem. Phys.* **2020**, *152*, 224108.

(83) Neese, F. Software update: The ORCA program system–Version 5.0. *WIREs Comput Mol Sci* **2022**, *12*, e1606.

(84) Knowles, P. J.; Hampel, C.; Werner, H.-J. Coupled cluster theory for high spin, open shell reference wave functions. *J. Chem. Phys.* **1993**, *99*, 5219–5227.

(85) Watts, J. D.; Gauss, J.; Bartlett, R. J. Coupled-cluster methods with noniterative triple excitations for restricted open-shell Hartree–Fock and other general single determinant reference functions. Energies and analytical gradients. *J. Chem. Phys.* **1993**, *98*, 8718–8733.

(86) Shamasundar, K. R.; Knizia, G.; Werner, H.-J. A new internally contracted multi-reference configuration interaction method. *J. Chem. Phys.* **2011**, *135*, 054101.

(87) MOLPRO, versions 2015–2023, a package of ab initio programs, H.-J. Werner, P. J. Knowles, and others, see `https://www.molpro.net`.

(88) Werner, H.-J.; Knowles, P. J.; Knizia, G.; Manby, F. R.; Schütz, M. Molpro: A General-Purpose Quantum Chemistry Program Package. *WIREs Comput. Mol. Sci.* **2012**, *2*, 242–253.

(89) Werner, H.-J. et al. The Molpro quantum chemistry package. *J. Chem. Phys.* **2020**, *152*, 144107.

(90) Aquilante, F. et al. Modern quantum chemistry with [Open]Molcas. *J. Chem. Phys.* **2020**, *152*, 214117.

(91) Knizia, G.; Adler, T. B.; Werner, H.-J. Simplified CCSD(T)-F12 methods: Theory and benchmarks. *J. Chem. Phys.* **2009**, *130*, 054104.

(92) Pierloot, K. The CASPT2 Method in Inorganic Electronic Spectroscopy: From Ionic Transition Metal to Covalent Actinide Complexes. *Mol. Phys.* **2003**, *101*, 2083–2094.

(93) Pierloot, K. Transition Metals Compounds: Outstanding Challenges for Multiconfigurational Methods. *Int. J. Quantum Chem.* **2011**, *111*, 3291–3301.

(94) Ordejón, B.; de Graaf, C.; Sousa, C. Light-Induced Excited-State Spin Trapping in Tetrazole-Based Spin Crossover Systems. *J. Am. Chem. Soc.* **2008**, *130*, 13961–13968.

(95) Sousa, C.; de Graaf, C. *Spin States in Biochemistry and Inorganic Chemistry*; Wiley, 2015; pp 35–57.

(96) Pierloot, K.; Phung, Q. M.; Domingo, A. Spin State Energetics in First-Row Transition Metal Complexes: Contribution of (3s3p) Correlation and its Description by Second-Order Perturbation Theory. *J. Chem. Theory Comput.* **2017**, *13*, 537–553.

(97) Dose, E. V.; Murphy, K. M. M.; Wilson, L. J. Sythesis and Spin-State Studies in Solution of γ-Substituted Tris(β-deketonato)iron(III) Complexes and Their Spin-Equilibrium

β-Ketoimine Analogues Dervied from Triethylenetetramine. *Inorg. Chem.* **1976**, *15*, 2622–2630.

(98) Pyykkönen, A.; Feher, R.; Köhler, F. H.; Vaara, J. Paramagnetic Pyrazolylborate Complexes Tp2M and Tp*2M: 1H, 13C, 11B, and 14N NMR Spectra and First-Principles Studies of Chemical Shifts. *Inorg. Chem.* **2020**, *59*, 9294–9307.

(99) Rat, S.; Ridier, K.; Vendier, L.; Molnár, G.; Salmon, L.; Bousseksou, A. Solvatomorphism and structural-spin crossover property relationship in bis[hydrotris(1,2,4-triazol-1-yl)borate]iron(ii). *CrystEngComm* **2017**, *19*, 3271–3280.

(100) Turner, J. W.; Schultz, F. A. Intramolecular and Environmental Contributions to Electrode Half-Reaction Entropies of M(tacn)23+/2+ (M = Fe, Co, Ni, Ru; tacn = 1,4,7-Triazacyclononane) Redox Couples. *Inorg. Chem.* **1999**, *38*, 358–364.

(101) Turner, J. W.; ; Schultz, F. A. Solution Characterization of the Iron(II) Bis(1,4,7-Triazacyclononane) Spin-Equilibrium Reaction. *Inorg. Chem.* **2001**, *40*, 5296–5298.

(102) Holland, J. M.; McAllister, J. A.; Lu, Z.; Kilner, C. A.; Thornton-Pett, M.; Halcrow, M. A. An unusual abrupt thermal spin-state transition in [FeL][BF] [L = 2,6-di(pyrazol-1-yl)pyridine]. *Chem. Commun.* **2001**, 577–578.

(103) Holland, J. M.; McAllister, J. A.; Kilner, C. A.; Thornton-Pett, M.; Bridgeman, A. J.; Halcrow, M. A. Stereochemical effects on the spin-state transition shown by salts of [FeL2]2+ [L = 2,6-di(pyrazol-1-yl)pyridine]. *J. Chem. Soc., Dalton Trans.* **2002**, 548–554.

(104) Li, J.; Peng, Q.; Barabanschikov, A.; Pavlik, J. W.; Alp, E. E.; Sturhahn, W.; Zhao, J.; Sage, J. T.; Scheidt, W. R. Vibrational Probes and Determinants of the $S = 0 \leftrightarrows S = 2$ Spin Crossover in Five-Coordinate $[Fe(TPP)(CN)]^{-}$. *Inorg. Chem.* **2012**, *51*, 11769–11778.

(105) Simmons, M. G.; Wilson, L. J. Magnetic and Spin Lifetime Studies in Solu-

tion of a $\Delta S = 1$ Spin-Equilibrium Process for Some Six-Coordinate Bis(*N*-R-2,6-pyridinedicarboxaldimine)cobalt(II) Complexes. *Inorg. Chem.* **1977**, *16*, 126–130.

(106) Smith, M. E.; Andersen, R. A. $Me_5C_5Ni(acac)$: A Monomeric, Paramagnetic, 18-Electron, Spin-Equilibrium Molecule. *J. Am. Chem. Soc.* **1996**, *118*, 11119–11128.

(107) Koehler, F. H.; Schlesinger, B. Spin crossover, dimerization, and structural dynamics of manganocenes probed by deuterium NMR spectroscopy. *Inorg. Chem.* **1992**, *31*, 2853–2859.

(108) Schmidtke, H.-H.; Eyring, G. The Cation Effect on the Charge Transfer and Ligand Field Spectrum of the Complex Ferricyanide. *Zeitschrift für Physikalische Chemie* **1974**, *92*, 211–222.

(109) Li, J.; Lord, R.; Noll, B.; Baik, M.-H.; Schulz, C.; Scheidt, W. Cyanide: A Strong-Field Ligand for Ferrohemes and Hemoproteins? *Angew. Chem. Int. Ed.* **2008**, *47*, 10144–10146.

(110) Juhász, G.; Hayami, S.; Inoue, K.; Maeda, Y. $[CoII(phimpy)_2](ClO_4)_2$ and $[CoII(ipimpy)_2](ClO_4)_2$: New Cobalt(II) Spin Crossover Compounds, and the Role of the Ligand Flexibility in Spin Transition Behavior. *Chem. Lett.* **2003**, *32*, 882–883.

(111) Morioka, Y.; Toriumi, K.; Ito, T.; Saito, A.; Nakagawa, I. Crystal Structures of the Room- and Low-Temperature Phases of Monoclinic Potassium Ferricyanide. *J. Phys. Soc. Japan* **1985**, *54*, 2184–2189.

(112) Willans, M. J.; Wasylishen, R. E.; McDonald, R. Polymorphism of Potassium Ferrocyanide Trihydrate as Studied by Solid-State Multinuclear NMR Spectroscopy and X-ray Diffraction. *Inorg. Chem.* **2009**, *48*, 4342–4353.

(113) Ueda, T.; Bernard, G. M.; McDonald, R.; Wasylishen, R. E. Cobalt-59 NMR and X-ray diffraction studies of hydrated and dehydrated (±)-tris(ethylenediamine) cobalt(III) chloride. *Solid State Nucl. Magn. Res.* **2003**, *24*, 163–183.

(114) Krüger, G. J.; Reynhardt, E. C. New investigation of the structure of trisacetylacetonatocobalt(III). *Acta Crystallographica Section B* **1974**, *30*, 822–824.

(115) Diaz-Acosta, I.; Baker, J.; Cordes, W.; Pulay, P. Calculated and Experimental Geometries and Infrared Spectra of Metal Tris-Acetylacetonates: Vibrational Spectroscopy as a Probe of Molecular Structure for Ionic Complexes. Part I. *J. Phys. Chem. A* **2001**, *105*, 238–244.

(116) Junk, P. C. Supramolecular interactions in the X-ray crystal structure of potassium tris(oxalato)ferrate(III) trihydrate. *J. Coord. Chem.* **2005**, *58*, 355–361.

(117) Montgomery, H.; Morosin, B.; Natt, J. J.; Witkowska, A. M.; Lingafelter, E. C. The crystal structure of Tutton's salts. VI. Vanadium(II), iron(II) and cobalt(II) ammonium sulfate hexahydrates. *Acta Crystallographica* **1967**, *22*, 775–780.

(118) Kepp, K. P. Consistent descriptions of metal–ligand bonds and spin-crossover in inorganic chemistry. *Coord. Chem. Rev.* **2013**, *257*, 196–209.

(119) Sorai, M. In *Spin Crossover in Transition Metal Compounds III*; Gütlich, P., Goodwin, H. A., Eds.; Springer: Berlin, Heidelberg, 2004; pp 153–170.

(120) Radoń, M. Predicting Spin States of Iron Porphyrins with DFT Methods Including Crystal Packing Effects and Thermodynamic Corrections. *Phys. Chem. Chem. Phys.* **2024**, *26*, 18182–18195.

(121) Tanabe, Y.; Sugano, S. On the Absorption Spectra of Complex Ions II. *J. Phys. Soc. Japan* **1954**, *9*, 766–779.

(122) Neese, F. In *Practical Approaches to Biological Inorganic Chemistry*; Crichton, R. R., Louro, R. O., Eds.; Elsevier: Oxford, 2013; pp 23 – 51.

(123) Avila Ferrer, F. J.; Cerezo, J.; Stendardo, E.; Improta, R.; Santoro, F. Insights for an Accurate Comparison of Computational Data to Experimental Absorption and Emission Spectra:

Beyond the Vertical Transition Approximation. *J. Chem. Theory Comput.* **2013**, *9*, 2072–2082.

(124) Bai, S.; Mansour, R.; Stojanović, L.; Toldo, J. M.; Barbatti, M. On the origin of the shift between vertical excitation and band maximum in molecular photoabsorption. *Journal of Molecular Modeling* **2020**, *26*, 107.

(125) Pierloot, K.; Praet, E. V.; Vanquickenborne, L. G.; Roos, B. O. Systematic ab initio study of the ligand field spectra of hexacyanometalate complexes. *J. Phys. Chem.* **1993**, *97*, 12220–12228.

(126) Derenzo, S. E.; Klintenberg, M. K.; Weber, M. J. Determining point charge arrays that produce accurate ionic crystal fields for atomic cluster calculations. *J. Chem. Phys.* **2000**, *112*, 2074.

(127) Hocking, R. K.; Wasinger, E. C.; de Groot, F. M. F.; Hodgson, K. O.; Hedman, B.; Solomon, E. I. Fe L-Edge XAS Studies of $K_4[Fe(CN)_6]$ and $K_3[Fe(CN)_6]$: A Direct Probe of Back-Bonding. *J. Am. Chem. Soc.* **2006**, *128*, 10442–10451.

(128) Avila, M.; Torres, L.; Montero-Alejo, A. L.; Reguera, L.; Reguera, E. On the $CN^{-}\cdots K$ coordination modes in $K_n[M^{6-n}(CN)_6]\cdot xH_2O$: first evidence of $CN^{-}\cdots K$ electron-deficient bonding. *Dalton Trans.* **2021**, *50*, 2510–2520.

(129) Renovitch, G. A.; Baker, W. A. Magnetic and spectral properties of [Fe(en)3]Cl3. *J. Am. Chem. Soc.* **1968**, *90*, 3585–3587.

(130) Jørgensen, C. Absorption spectrum of manganese (II) diethylenetriamine complexes. *Inorg. Chim. Acta* **1969**, *3*, 313–314.

(131) Pham, D. N. K.; Roy, M.; Golen, J. A.; Manke, D. R. The first-row transition-metal series of tris(ethylenediamine) diacetate complexes $[M(en)_3](OAc)_2$ (*M* is Mn, Fe, Co, Ni, Cu, and Zn). *Acta Cryst. C* **2017**, *73*, 442–446.

(132) Chen, X.; Xue, C.; Liu, S.-X.; Liu, J.-L.; Yao, Z.-Y.; Ren, X.-M. Fluorite-type coordination compound as iodide ion conductor: crystal structure and ionic conductivity. *Dalton Trans.* **2017**, *46*, 12916–12922.

(133) Feldt, M.; Phung, Q. M.; Pierloot, K.; Mata, R. A.; Harvey, J. N. Limits of Coupled-Cluster Calculations for Non-Heme Iron Complexes. *J. Chem. Theory Comput.* **2019**, *15*, 922–937.

(134) Fang, Z.; Vasiliu, M.; Peterson, K. A.; Dixon, D. A. Prediction of Bond Dissociation Energies/Heat of Formation for Diatomic Transition metal Compounds: CCSD(T) Works. *J. Chem. Theory Comput.* **2017**, *13*, 1057–1066.

(135) Aðalsteinsson, H. M.; Bjornsson, R. Ionization energies of metallocenes: a coupled cluster study of cobaltocene. *Phys. Chem. Chem. Phys.* **2023**, *25*, 4570–4587.

(136) Benedek, Z.; Timár, P.; Szilvási, T.; Barcza, G. Sensitivity of coupled cluster electronic properties on the reference determinant: Can Kohn-Sham orbitals be more beneficial than Hartree-Fock orbitals? *J Comput Chem* **2022**, *43*, 2103–2120.

(137) Drosou, M.; Mitsopoulou, C. A.; Pantazis, D. A. Spin-State Energetics of Manganese Spin Crossover Complexes: Comparison of Single-Reference and Multi-Reference Ab Initio Approaches. *Polyhedron* **2021**, 115399.

(138) Szalay, P. G.; Müller, T.; Gidofalvi, G.; Lischka, H.; Shepard, R. Multiconfiguration Self-Consistent Field and Multireference Configuration Interaction Methods and Applications. *Chem. Rev.* **2012**, *112*, 108–181.

(139) Arbuznikov, A. V.; Kaupp, M. Towards improved local hybrid functionals by calibration of exchange-energy densities. *J. Chem. Phys.* **2014**, *141*, 204101.

(140) Vydrov, O. A.; Scuseria, G. E.; Perdew, J. P. Tests of functionals for systems with fractional electron number. *J. Chem. Phys.* **2007**, *126*, 154109.

(141) Zhao, Y.; Truhlar, D. G. The M06 Suite of Density Functionals for Main Group Thermochemistry, Thermochemical Kinetics, Noncovalent Interactions, Excited States, and Transition Elements: Two New Functionals and Systematic Testing of Four M06-class Functionals and 12 Other Functionals. *Theor. Chem. Acc.* **2008**, *120*, 215–241.

(142) Mardirossian, N.; Head-Gordon, M. ωB97X-V: A 10-parameter, range-separated hybrid, generalized gradient approximation density functional with nonlocal correlation, designed by a survival-of-the-fittest strategy. *Phys. Chem. Chem. Phys.* **2014**, *16*, 9904–9924.

(143) Swart, M.; Solá, M.; Bickelhaupt, F. M. A new all-round density functional based on spin states and SN2 barriers. *J. Chem. Phys.* **2009**, *131*, 094103.

(144) Neugebauer, H.; Bädorf, B.; Ehlert, S.; Hansen, A.; Grimme, S. High-throughput screening of spin states for transition metal complexes with spin-polarized extended tight-binding methods. *J. Comput. Chem.* **2023**, *44*, 2120.

(145) Siegbahn, P. E. M.; Himo, F. The quantum chemical cluster approach for modeling enzyme reactions. *WIREs Comput. Mol. Sci.* **2011**, *1*, 323–336.

(146) Mata, R. A.; Suhm, M. A. Benchmarking Quantum Chemical Methods: Are We Heading in the Right Direction? *Angew. Chem. Int. Ed.* **2017**, *56*, 11011–11018.

TOC Graphic